

Master Thesis

Fluorescence Image Based
Food Quality Measurement

蛍光画像解析に基づく食品品質検査



Dept. of Information & Communications Engineering
Grad. Sch. of Information Science and Technology
The University of Tokyo

48-126449

Meng Wang

Advisor Professor Yoichi Sato

February 2014

Fluorescence Image Based Food Quality Measurement

Copyright © 2014

by

Meng Wang

Abstract

Computer vision method has been widely used in food quality measurement to save time and cost, such as hyperspectral imaging, EEM spectra, etc. However, all these methods are either quite time consuming or of high requirement for equipment, which is not convenient enough. On the other hand, some previous research has indicated that food quality is highly correlated to the fluorescence they emit.

In this thesis, we proposed a fluorescence image based method to measure food quality. Through survey, we focus on a few primary fluorescent components that widely exist in food, such as NADH and tryptophan. Aiming at the Excitation-Emission spectra of these components, we use corresponding light source and filters to get their fluorescence images. We successfully observed fluorescence from meat in the middle range of visible wavelengths and buckwheat flour at 650 nm. We also did experiment on both dried buckwheat noodles and boiled buckwheat noodles, finding that fluorescence of buckwheat can also be observed from them by using suitable light source and filters at 650 nm. It means that predicting buckwheat content in cooked commercial buckwheat products by using fluorescence images is feasible.

Further more, we take fluorescence images of a mixed powder of buckwheat flour and wheat flour at 6 different wavelengths between 400 nm and 700 nm, then use PLS regression analysis to estimate the ratio of buckwheat with the best result $R^2 = 0.986679$ and $SEP = 0.131205$. The result shows that our method is applicable for detecting buckwheat flour ratio in a mixture of wheat and buckwheat flours easily and rapidly, and potential for detecting buckwheat ratio in commercial buckwheat products. Since the primary fluorescence components in different kinds of food are nearly the same, this method is a very promising approach to measure the quality of varies kinds of foods.

Acknowledgement

I would like to express my sincere gratitude to all those who have helped me complete this thesis in the past two years.

First, I would like to express my deepest appreciation to my research advisors, Professor Yoichi Sato and Imari Sato, for their kind guidance and strong supports on my research. Sato Sensei's kindness has always brought me great confidence on both study and life. Thanks to Imari Sensei's novel ideas, this work carried on smoothly. Without their guidance and persistent help, this thesis would not have been possible.

Next, I would like to thank Mr. Lu Feng and Mr. Antony Lam, who have given me many instructions on research and have taught me a lot about the techniques of experiments. Mr Antony also encouraged me a lot when I met with difficulties during this work.

I also appreciate Mr. Tetsu Matsukawa for examining and approving my thesis. It is he who told me that there was a grammatical mistake in the Japanese title of my thesis, and suggested me to modify it.

At the same time, I wish to express my thanks to all Sato Laboratory staffs and members. It is all the members in this laboratory that made my two years study in the University of Tokyo a wonderful time.

Last but not least, I want to thank my parents, for their persistent encouragement and assistance in the past two years. Thanks them for understanding that I haven't returned home for once since I came to Japan.

6th February, 2014

Meng Wang

Table of Contents

Abstract

Acknowledgement

Chapter 1: Introduction	1
1.1 Background	1
1.2 Purpose of Research	5
1.3 Thesis Overview	5
Chapter 2: Related Research on Food Quality Measurement	6
2.1 Typical Image Based Method	6
2.2 Hyperspectral Imaging Based Method	10
2.3 Fluorescence Spectra Based Method	13
Chapter 3: Fluorescence and Food Quality	15
3.1 Properties of Fluorescence	15
3.2 Fluorophores in Food	18
3.3 Fluorescence and Food Quality	22
Chapter 4: Proposed Method	26
4.1 The Model of Reflective and Fluorescent Components in an Image	26
4.2 Observation of Fluorescence	27
4.3 Estimation of Buckwheat Flour	28
Chapter 5: Experiments	31
5.1 Materials	31
5.2 Image Acquisition and Preprocessing	32
5.3 Estimation of Buckwheat Flour Ratio	34
5.4 Observation of Fluorescence	36
Chapter 6: Conclusion	41
6.1 Summary	41
6.2 Discussion and Future Works	42
References	43

List of Figures and Tables

List of Figures

1.1	Schematic diagram of hyperspectral image for a piece of meat showing the relationship between spectral and spatial dimensions. [1]	2
1.2	Synchronous Fluorescence Spectra of Cereal Flours [2].	3
2.1	The saturation images of two samples of different tenderness exhibit different image textures. The left sample is less tender.	7
2.2	The direction () of pixel pairs and the distance (d) between the pixel pairs used to construct the grey level co-occurrence matrix. (a) Illustration of direction () and distance (d) in images of pixel pairs (x1, y2) and (x2, y2); (b) (e) four examples at direction 0, 45, 90, and 135 °, respectively [3].	8
2.3	Pixels of a colour image of round slices from cooked beef joints in RGB spaces [4].	9
2.4	Schematic diagram of the main components of the hyperspectral imaging system [5].	10
2.5	Concentration maps for minced pork samples with predicted composition (%): (a) pseudo-colour image composed by three selected wavelengths (1081 nm, 1275 nm, 1329 nm), (b) concentration map for fat.	11
2.6	Acquired hyperspectral images, the colored images were obtained by combined images at wavelengths of 460 nm, 580 nm and 720 nm. PSE, PFN, RFN and RSE are 4 kinds of pork quality subjectively determined by people based on the color, texture and exudation of meat.	12
2.7	Weights of the first three principle components at different wavelength. Upper: weights of average reflectance spectrum; Lower: weights of the first derivative of the average reflectance spectrum.	12
2.8	Measured EEM fluorescence spectra at 0 h (left) and 72 h (right). Horizontal axis shows the emission wavelength; vertical axis shows the excitation wavelength; color bar indicates the fluorescence intensity.	14
2.9	Viable bacteria distributions. Left to right: viable bacteria images at 0 h, 24 h, 48 h, and 72 h after the pork piece was cut.	14
3.1	Principle of Fluorescence	15

3.2	An example of absorption and emission spectra [6].	16
3.3	The fluorescence on the surface of banana [7].	18
3.4	Excitation and emission spectra of the 11 fluorophores.	20
3.5	Excitation-Emission Matrix of the 11 fluorophores.	21
3.6	EE spectra changes as meat being cooked.	23
3.7	Excitation spectra of 4 primary fluorophores in meat.	24
3.8	Emission spectra of 4 primary fluorophores in meat.	24
3.9	Fluorescence spectra of pork meat stored under different temperature measured at different storage times.	25
4.1	Photographic method and principle of catching fluorescence. In the formula, p_a represents the image taken only under ambient light. p_f represents the image of fluorescence component. p_{uv} represents the image of UV component.	27
4.2	EEM of buckwheat flour (left) and wheat flour (right).	28
4.3	Schematic flow of the proposed method.	29
5.1	4 kinds of materials.	31
5.2	The imaging system in our experiments.	33
5.3	Example of 6 spectral images of a flour sample after preprocessing. Upper row of images were taken under ambient light. Lower row was taken under ambient plus 370 nm UV light.	33
5.4	Changes of SEP with the number of latent variables.	34
5.5	Relationship between true and predicted buckwheat flour ratios. Black spots represent calibration set, while red triangle represent validation set.	35
5.6	Fluorescence images of pork meat.	37
5.7	Images of dried noodles taken at 650nm. From top to bottom: 100% buckwheat noodle, 80% buckwheat noodle, 50% buckwheat noodle, Udon and Pasta. Images in the left colume were taken under ambient light, while the middle colume were taken under ambient and UV light.	38
5.8	Images of boiled noodles taken at 650nm. From top to bottom: 100% buckwheat noodle, 80% buckwheat noodle, 50% buckwheat noodle, Udon and Pasta. Images in the left colume were taken under ambient light, while the middle colume were taken under ambient and UV light.	39
5.9	Fluorescence images of dried noodles taken at 650 nm. Images in the top row were taken by using 370 nm UV light source, while images in the second row were taken by using ordinary blue light.	40
5.10	Fluorescence images of boiled noodles taken at 650 nm. Images in the top row were taken by using 370 nm UV light source, while images in the second row were taken by using ordinary blue light.	40

List of Tables

3.1	List of 11 food-relevant fluorophores and their fluorescent properties. (Data from the food fluorescence database at www.models.kvl.dk .)	19
5.1	Statistics of the prediction result of 4 dataset combinations.	35
5.2	Comparison of previous and our method.	36
5.3	Comparison result on data group 1.	36
5.4	Comparison result on data group 2.	36

Chapter 1

Introduction

1.1 Background

With the abundance of daily food in variety and amount, people make choices about food quality every day by choosing from a large number of samples in the market. However, there are more and more food quality problems that worried us at the same time. For example: thawed meat is wrong labeled and sold as fresh meat [8, 9], buckwheat noodles adulterated with more wheat flour than the regulated amount are sold [10], and so on. Fraudulent labeling of food products to sell at an inflated price has become a social problem all around the world. In order to prevent food retailers from providing food of bad qualities, several methods have been proposed to measure the quality of different kinds of food.

Take meat for example, traditional methods that rely on electrical properties [11], enzyme activity determination [12], and sensory changes [9] are usually used in industry and processing lines. However, these methods often require complex treatments and skilled technicians. A simple, rapid and non-destructive method for predicting food quality is necessary.

Recently, computer vision method based on the analysis of digital images are widely used for visual evaluation of meat joints and cuts [13]. This technique is based on the analysis of spatial information acquired from the digital image of an object, which includes geometrical, size, appearance, and color features. The exhibility and the non-destructive nature of this technique make it popular in the food industry [14, 15]. Unfortunately, this method is most effective when quality attributes of food are related to its extrinsic characteristics, but it becomes less effective or ineffective when quality attributes are mainly determined by the intrinsic properties of the product, such as composition and internal physical characteristics, which are not detectable from the surface [16]. Analogously,

near-infrared spectroscopy (NIRS) techniques have also received considerable attention as it has the potential of simultaneously measuring multiple quality attributes in a fast and non-destructive way. However, although this method is possible to obtain compositional information of food products based on the spectral features of the samples, it is difficult to know the location of such information due to its limited spatial resolution [17, 18].

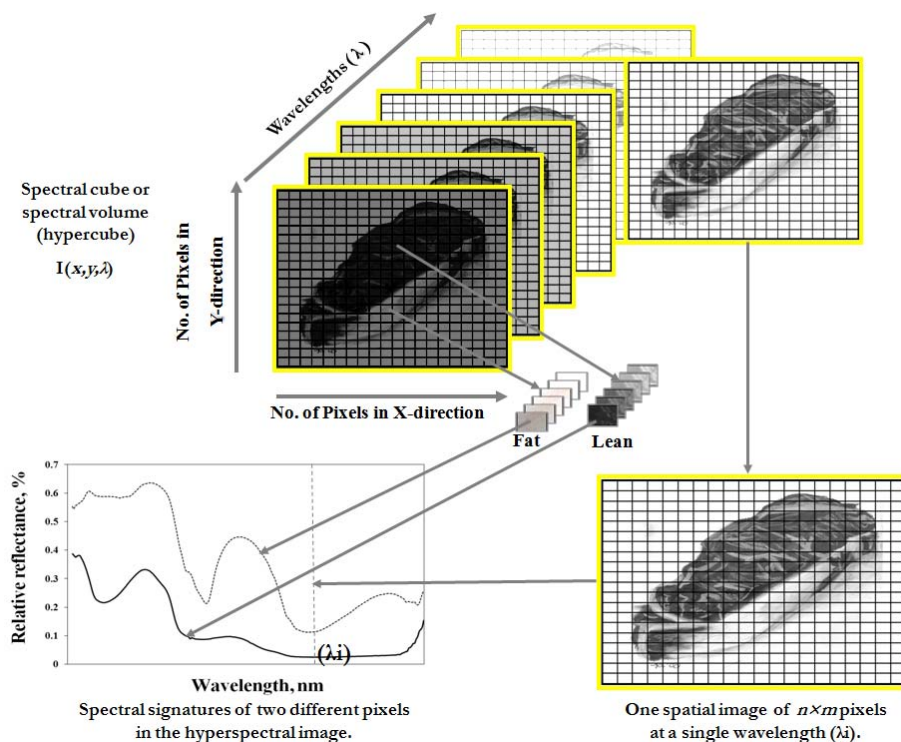


Figure 1.1: Schematic diagram of hyperspectral image for a piece of meat showing the relationship between spectral and spatial dimensions. [1]

Hyperspectral imaging is a rapid and non-destructive analytical technique that integrates both spectroscopic and imaging techniques in one system to provide both spectral and spatial information simultaneously. It provides spatial information, as regular imaging systems, along with spectral information for each point in the image as spectroscopic techniques. Figure 1.1 shows an example of the hyperspectral image for a piece of meat. In figure 1.1, every pixel in the hyperspectral image is represented by an individual spectrum containing information about chemical composition at this pixel. By combining the chemical selectivity of spectroscopy with the power of image visualization, hyperspectral imaging is particularly useful in situations where multiple quality attributes must be

considered and when either computer vision or spectroscopy is not suitable. However, hyperspectral imaging has a high requirement on equipment.

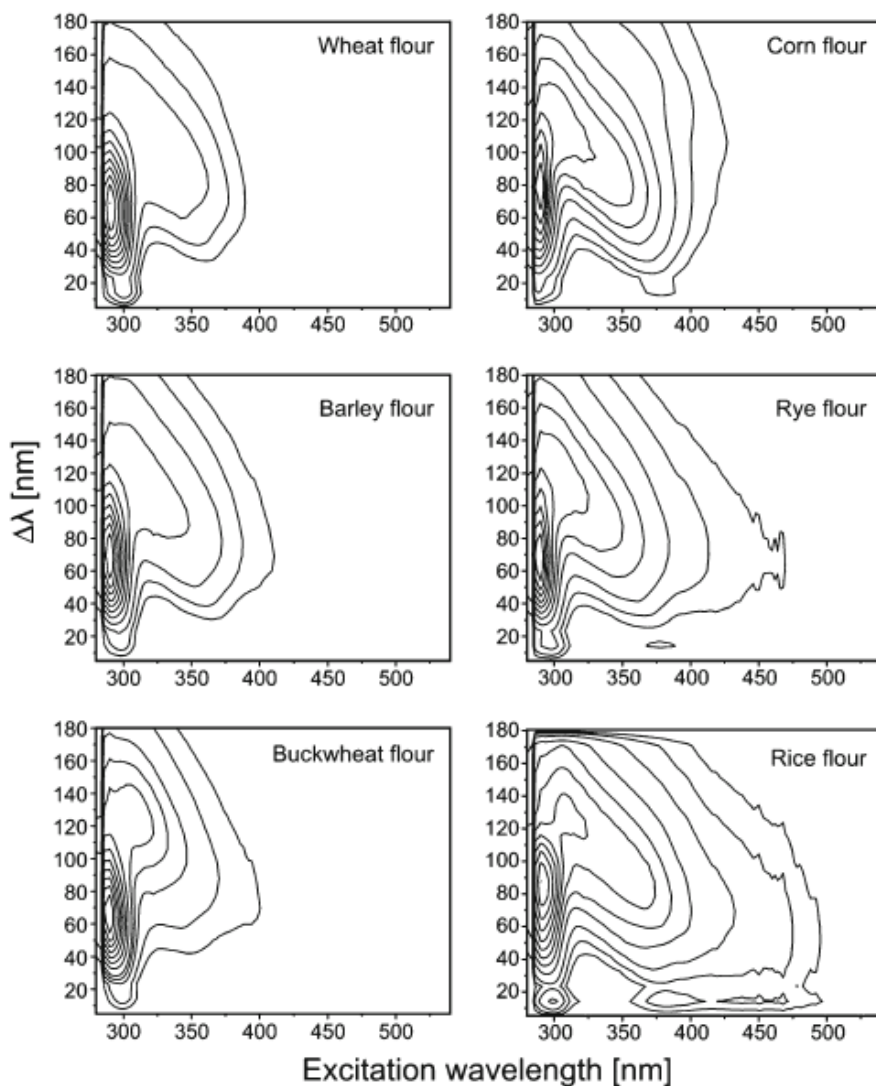


Figure 1.2: Synchronous Fluorescence Spectra of Cereal Flours [2].

On the other hand, since fluorescence is found to be related to food quality, various methods based on fluorescence are also proposed. Synchronous fluorescence spectroscopy, a technique that measures both the absorption and the emission properties of a sample in a single measurement, was used for food quality measurement. Since the measured spectrum is dependent on both the absorption and the emission characteristics of samples, this method can provide a large amount of information of food [2]. Figure 1.2 shows an example of SF spectrum. In the figure, vertical axis represents the constant

wavelength interval between Excitation and Emission wavelengths.

Analogously, the front-face fluorescence spectroscopy (FFFS) can almost be used to detect changes in any kinds of food [19]. The Excitation-Emission matrix (EEM) [20], also known as the fluorescence fingerprint (FF), is also used to identify certain constituents and visualize their distributions in foods [21–23]. But the greatest disadvantage of this kind method is that measuring spectra or EEM of food is quite time consuming, which is quite inconvenient.

Although various kinds of methods have been proposed, they are either of high requirement for equipment or time consuming. A more easier, rapid, and widely available food quality measurement is needed.

1.2 Purpose of Research

In this thesis, we propose a fluorescence image based method to measure food quality. Since fluorescence can be used to identify certain constituents and detect slight differences in foods, we try to find a more easier and convenient method that is based on fluorescence to measure food quality, especially some kinds of quality like freshness, specific component ratio, etc. Through survey, we focus on a few primary fluorescent components that widely exist in food, such as NADH and tryptophan. Aiming at the Excitation-Emission spectra of these components, we use corresponding light source to excite specific fluorescence component in food then select proper filters to catch their fluorescence images. We successfully catch the fluorescence of meat in FG channel and the fluorescence of buckwheat at 650nm. Then we take fluorescence images of a mixed powder of buckwheat flour and wheat flour in the same way at 6 wavelengths between 400nm and 700nm, and use PLS regression analysis to build prediction formula in 2 latent variables.

After that, we do the same thing on both dried commercial buckwheat noodles and boiled noodles, and present a new method to estimate the buckwheat ratio in noodles. According to our idea, this method is not only feasible, but also quite easier and rapid.

1.3 Thesis Overview

The rest of this thesis is organized as follows. In Chapter 2, some related works on image based food quality measurement are introduced. In Chapter 3, survey result on fluorescence components in food and the relationship between fluorescence and food quality are introduced. Then we introduce the proposed method in Chapter 4, followed with our experiment and results in Chapter 5. At last, we conclude with a summary on our works followed by some discussions on future works in Chapter 6.

Chapter 2

Related Research on Food Quality Measurement

There are many kinds of food quality measurement methods proposed by previous researches. Some of them base on digital image processing, some of them base on the properties of fluorescence. Each method owns unique advantages which make it work well on specific kinds of food.

This chapter focuses on introducing all kinds of food quality measurement methods. The first section introduces typical single image based image processing method. The second section introduces works on measuring food quality through hyperspectral image. The third section introduce methods of using front-face fluorescence spectra. The fourth section introduces the food quality measurement method that bases on EEM. In the last section, a summary of related works is given.

2.1 Typical Image Based Method

As for a typical application of computer vision in the food industry, it should be the image processing method. Images of food products are captured by using a computer system then saved, processed, and displayed in the form of pixels from which information stored can be extracted as image features to indicate food qualities. Generally speaking, 4 major kinds of features are widely used, they are colour, size, shape, and texture [24]. Results from previous studies have shown that all these four features contained important information required for food quality evaluation. Color is the intensity of pixels, while size reflects the number of pixels. Shape describes the boundary of food products. Texture is the dependency between pixels and their neighbouring pixels or the variation of pixel intensities. This four image features have been widely applied in various kinds of food

such as fruits, vegetables, meat, and fishes for detection and segmentation of surface defects [25, 26], prediction and characterization of chemical and physical properties [27, 28], and evaluation and determination of sensory characteristics [29, 30]. Among these four features, since size and shape are very easy to understand, we mainly introduce color and texture features.

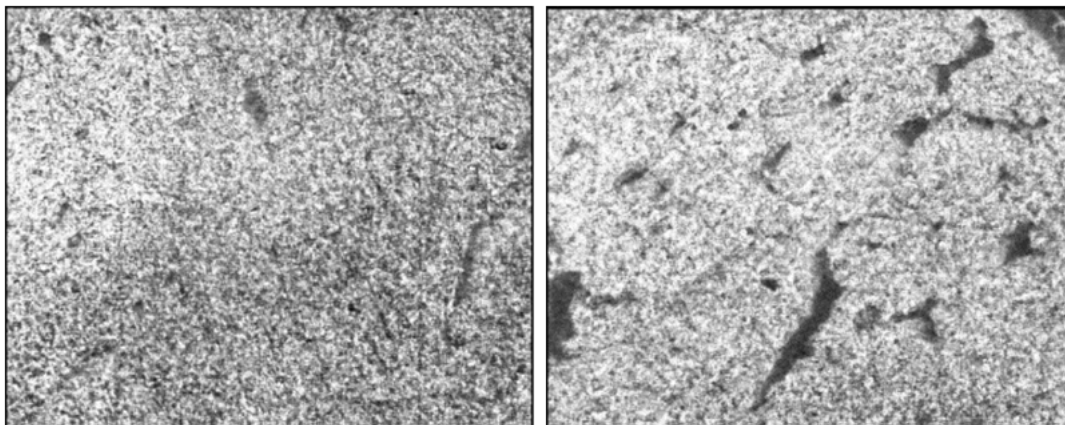


Figure 2.1: The saturation images of two samples of different tenderness exhibit different image textures. The left sample is less tender.

Texture feature

Texture features describe the textural patterns or properties of images, such as coarseness, fineness, granulation, randomness, lineation and so on [31]. These textural properties can explain the details of how the surfaces are composed of and structured by the dependency of pixels from each other or by the intensity variation across pixels, which corresponds to the way human percept food surface [32]. As a result, texture can generally be correlated to the sensory properties of food products [28, 29]. An example of texture features correlated to meat tenderness is shown in Figure 2.1 [33]. Besides, texture can also be used to determine chemical or physical properties of food products. It has been found that texture mostly contained more information about chemical and physical properties than colour and size [27].

The methods of extracting textures can be mainly categorized into four kinds as statistical texture, structural texture, model-based texture, and transform-based texture [3]. Among these four methods, a statistical texture analysis method named Grey level co-occurrence matrix is the mostly used, in which texture feature is extracted by some statistical approaches from the co-occurrence matrix, $p(k, l)$ [31]. The matrix is constructed by

counting the number of pixel pairs $(x_1, y_1)(x_2, y_2)$ with the grey value k and l at direction and distance d . An example for constructing the co-occurrence matrix is shown in Fig 2.2.

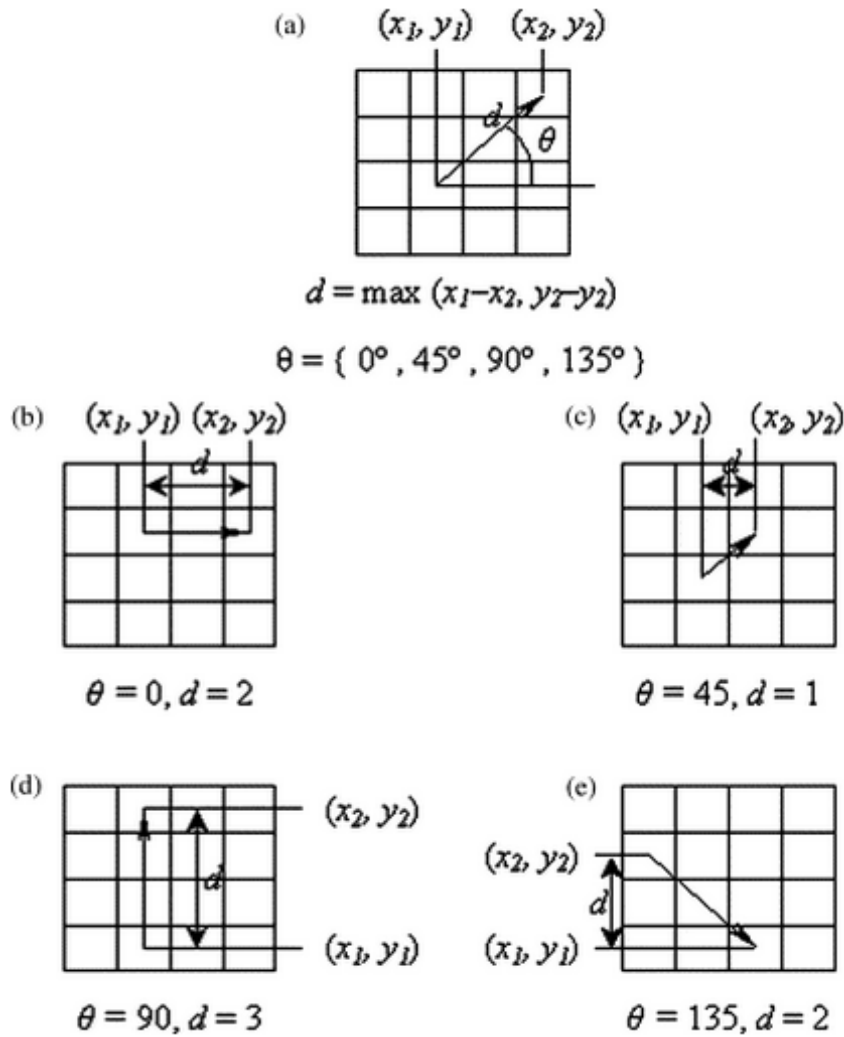


Figure 2.2: The direction () of pixel pairs and the distance (d) between the pixel pairs used to construct the grey level co-occurrence matrix. (a) Illustration of direction () and distance (d) in images of pixel pairs (x_1, y_1) and (x_2, y_2) ; (b) (e) four examples at direction 0, 45, 90, and 135 °, respectively [3].

Color feature

Color is one of the most important image features because it contains the basic information which is related to human vision. At the same time, color is the elementary information stored in pixels. A significant variation of color between two pixels in images generally indicates that the two pixels belong to different objects or different parts in an object with different characteristics. Under this consideration, color features can be used to detect defects in food products or to classify products having different qualities [34,35]. In general, images are stored in RGB color space where each pixel is composed of three integers ranging from 1 to 255 as illustrated in Fig 2.3. Besides RGB, some other color space are also often used, such as HSL, HSI, HSV and L*a*b.

However, since this method is based on image processing, it has a very high need on the quality of food images. To get a good measurement result, it is very important to select proper cameras and illumination to take perfect images first. As a result, this method has a very low usability. High requirement against photographic sets and illumination makes it only can be used in the factory, which bring little convenience to people's daily life.

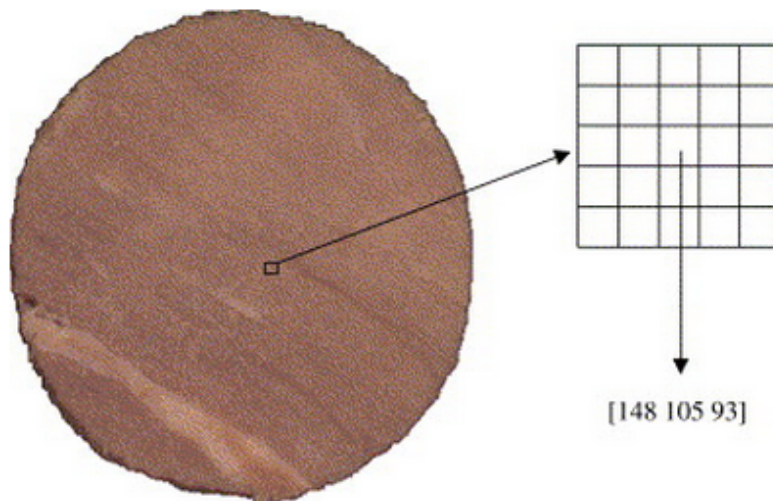


Figure 2.3: Pixels of a colour image of round slices from cooked beef joints in RGB spaces [4].

2.2 Hyperspectral Imaging Based Method

Hyperspectral imaging technique can provide not only spatial information but also spectral information of each pixel in an image. Such a wealth of information makes it can not only be used to detect physical characteristics such as color, size and texture, but also be used to extract intrinsic chemical and molecular information like water, fat and protein from a product. Recently, many hyperspectral images based food quality measurement method were proposed. For example, Cheng *et al.* developed a method to inspect damage of cucumber through hyperspectral images [36]. Another hyperspectral imaging system was developed to inspect the contamination of chicken carcasses [37, 38]. Besides, hyperspectra imaging has also been used for meat quality assessment, visualization of sugar distribution, classification of wheat kernels and so on [1].

A typical line-scan pushbroom hyperspectral imaging system is shown in Figure 2.4. The hyperspectral imaging system consists of a spectrograph, a camera, an illumination and a computer. Hyperspectral images of foods are taken as the conveyor move on.

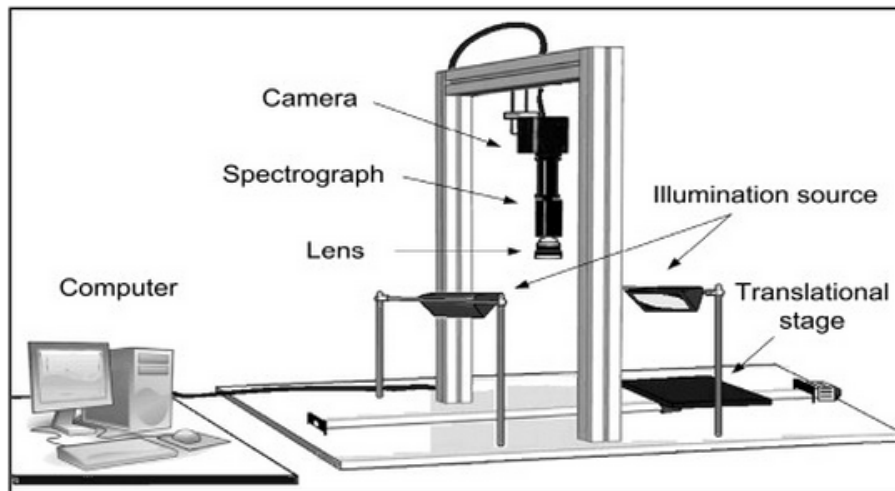


Figure 2.4: Schematic diagram of the main components of the hyperspectral imaging system [5].

Barbin *et al.* [39] used NIR hyperspectral imaging for fat quantification in minced pork. In their work, they also used a pushbroom hyperspectral imaging system in the reflectance mode. Near-infrared (NIR) hyperspectral images (900-1700 nm) were acquired and the mean spectra from the minced samples were extracted from the region of interest (ROI)

by doing a segmentation. Real fat content was measured by nuclear magnetic resonance (NMR). Partial least squares regression (PLSR) was used to build a model which correlated spectral information with fat content. Their result showed that combining NIR spectral data with cross-validated PLSR model together has a very good ability to predict fat content ($R^2=0.95$). Further more, they also applied the regression model obtained from selected wavelengths back to each pixel of spectral images to realize visualization. The result of visualization is shown in Figure 2.5.

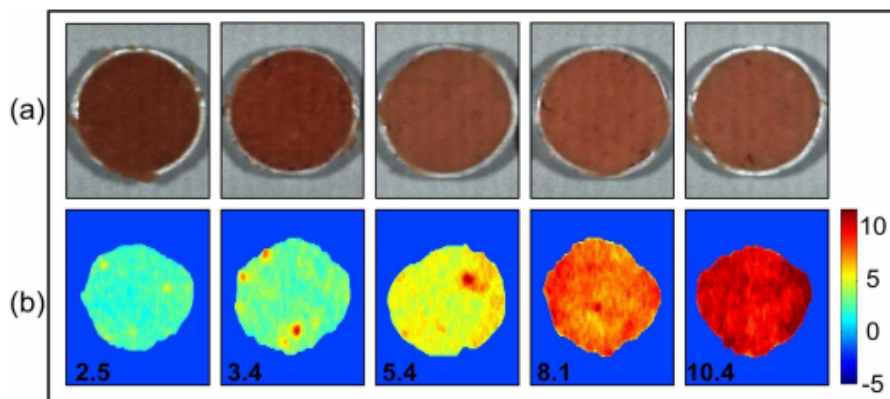


Figure 2.5: Concentration maps for minced pork samples with predicted composition (%): (a) pseudo-colour image composed by three selected wavelengths (1081 nm, 1275 nm, 1329 nm), (b) concentration map for fat.

Qiao Jun *et al.* [40] proposed a pork quality assessment method by using hyperspectral imaging technique. They first take hyperspectral images at a wavelength from 430 nm to 980 nm. An example of the meat images of 4 different qualities are shown in Figure 2.6. After pre-processing, they used principal component analysis (PCA) on both the average reflectance spectrum and the first derivative of the average reflectance spectrum to select a few feature wavebands from the entire spectral wavelengths (430 nm to 980 nm). Weights of the first three principle components are shown in figure 2.7. Then they used artificial neural network to classify pork into different quality groups. Finally PCA on the 1st derivative data gave the best classification result as 87.5% correction.

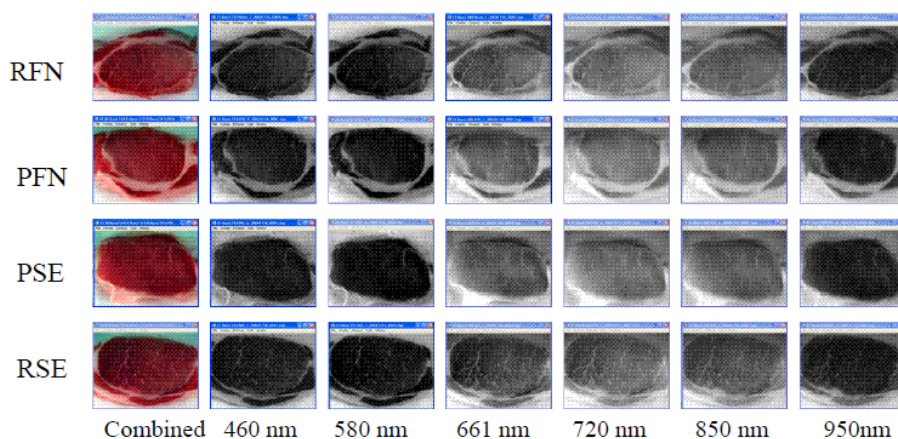


Figure 2.6: Acquired hyperspectral images, the colored images were obtained by combined images at wavelengths of 460 nm, 580 nm and 720 nm. PSE, PFN, RFN and RSE are 4 kinds of pork quality subjectively determined by people based on the color, texture and exudation of meat.

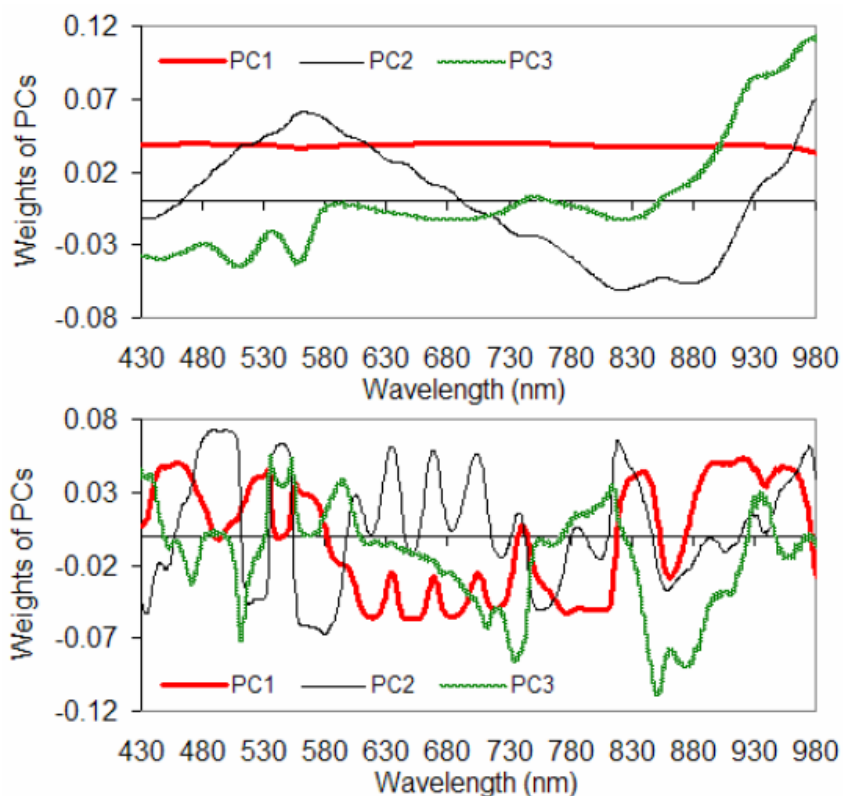


Figure 2.7: Weights of the first three principle components at different wavelength. Upper: weights of average reflectance spectrum; Lower: weights of the first derivative of the average reflectance spectrum.

2.3 Fluorescence Spectra Based Method

Fluorescence spectrum has been widely used to evaluate food quality. Although there are many previous research on food quality measurement using fluorescence, these methods can be divided into two kinds. One kind can be called Excitation-Emission spectra based method. A typical EE spectra based method is the front-face fluorescence spectra (FFFS) method, which is usually used to measure single fluorescent material in food. Since this method can focus on a specific single fluorescent component in food, it is widely used in all kinds of foods, such as dairy products, meat products, fish, fruits, vegetables and so on [19].

The other kind of method is based on the Excitation-Emission Matrix (EEM). The EEM is also called fluorescence fingerprint. It contains two-dimensional spectral data consisting of fluorescence spectrum and excitation spectrum. EEM has been widely used as a nondestructive method to measure physical and chemical properties of objects. It especially has greater potential than single fluorescence spectroscopy like FFFS when the object contains a few materials of different fluorescence characteristics. Therefore, EEM is effective for the identification and quantification of the composition of an object. Besides, EEM measurement technique has been expanded to EEM image measurement recently, which is similar to the evolution from spectrophotometry to hyperspectral imaging. Since EEM image is composed by fluorescence images of multiple excitation and emission wavelengths, it contains an EEM for each pixel. Tsuta *et al.* used EEM imaging to visualize the internal structure of soybean seeds [22]. Kokawa *et al.* showed that the gluten and starch distribution in dough can be visualized by EEM imaging [23].

However, measuring full EEM is quite time consuming. Nishino-san proposed a method to reduce the dimensions of EEM by designing optical combination of excitation-emission band-pass filters. According to their work, the output signals O_i of camera equipped with the i -th filter can be computed by the Equation below:

$$O_i = \int_{\lambda_{em}} \int_{\lambda_{ex}} T_i(\lambda_{ex}, \lambda_{em}) P(\lambda_{ex}) F(\lambda_{ex}, \lambda_{em}) S(\lambda_{em}) d\lambda_{ex} d\lambda_{em}, \quad (2.1)$$

where $T_i(\lambda_{ex}, \lambda_{em})$ is the two-dimensional transmittance function, $P(\lambda_{ex})$ is the spectral radiance of the excitation light, $F(\lambda_{ex}, \lambda_{em})$ are the EEM of the target, $S(\lambda_{em})$ is the spectral sensitivity of camera. Multivariate regression was used to establish a standard

curve by using the camera output signal vector as follow:

$$\hat{Y} = a_0 + a_1O_1 + a_2O_2 + \dots + a_NO_N, \quad (2.2)$$

where \hat{Y} is the estimated value, and a_0, a_1, \dots, a_N are the coefficients determined by the least square method. Estimation accuracy was evaluated using the standard error of prediction (SEP). They first collected EEM data from meat surface to compute O_i , and used chemical method to measure bacteria counts as Y . Thus optimal filter combinations are designed by maximize the estimation accuracy. An example of the EEM data in their work is shown in Figure 2.8 [41].

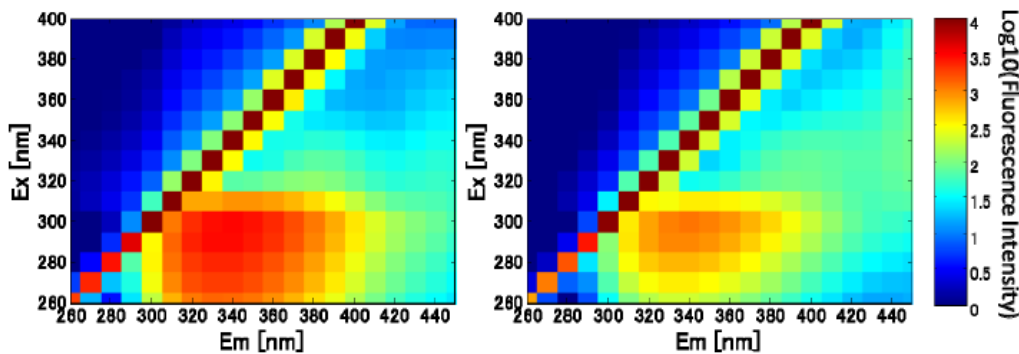


Figure 2.8: Measured EEM fluorescence spectra at 0 h (left) and 72 h (right). Horizontal axis shows the emission wavelength; vertical axis shows the excitation wavelength; color bar indicates the fluorescence intensity.

After getting optimal filter combinations, they take EEM images under these wavelengths to verify their method. At last, they applied this method to the quantification and visualization of bacteria on the surface of pork meat. The result is shown in Figure 2.9 [41].

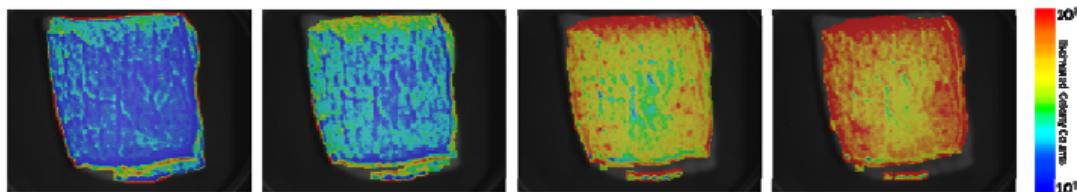


Figure 2.9: Viable bacteria distributions. Left to right: viable bacteria images at 0 h, 24 h, 48 h, and 72 h after the pork piece was cut.

Chapter 3

Fluorescence and Food Quality

In this section, we will discuss about some details on food and fluorescence. We start by introducing what fluorescence is and what kind of properties fluorescence has. Then we summarize some principle food-relevant fluorophores in all kinds of food, such as NADH, tryptophan, etc. These fluorophores are just the media for us to measure food quality through fluorescence images. We will also introduce some related research on food quality measurement using food fluorescence.

3.1 Properties of Fluorescence

Fluorescence emission is a common phenomenon occurring in many objects, such as natural gems and corals, uorescent dyes used for clothing, plant containing chlorophyll and so on. Fluorescence occurs when an orbital electron of a molecule or atom relaxes to its ground state by emitting a photon of light after being excited to a higher quantum state by some type of energy.

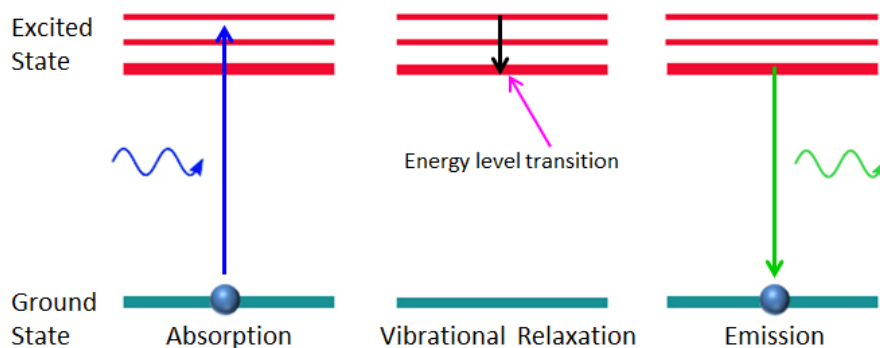


Figure 3.1: Principle of Fluorescence

Simply speaking, after an electron absorbs high energy, it is excited and begins jumping between different energy level vibrationally, and eventually fluoresces. The whole physics process is illustrated by the electronic-state diagram shown in Figure 3.1.

In general, when a reflecting material is illuminated by incident light, it reflects back light of the same wavelength. However, fluorescent materials on the contrary, first absorb incident light and then emit at longer wavelengths. This wavelength shifting property is known as Stokes Shift [42].

The Stokes Shift means that fluorescence owns two properties. One is that the color appearance of fluorescence is unaffected by incident illumination where it differs from ordinary reflectance. The second property is that fluorescent materials absorb light at a certain wavelength then reemit it at longer wavelengths after several nanoseconds, whereas ordinary reactive components reflect light at the same wavelength as incident illumination. As to which wavelengths of light are absorbed and which wavelengths are emitted, they are defined by the absorption and emission spectrum of fluorescent materials(Figure 3.2).

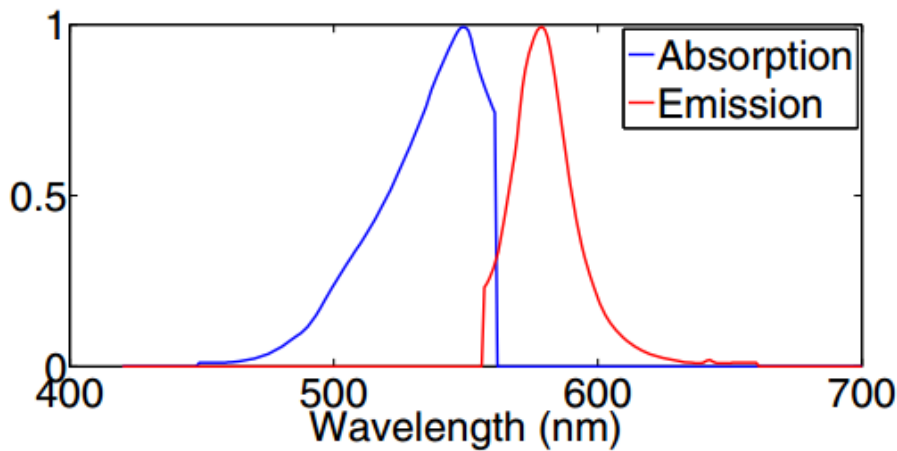


Figure 3.2: An example of absorption and emission spectra [6].

Moreover, due to these two unique properties, the appearance of fluorescent material is also computed in a different way from reflecting material. As we know, the color of reflecting material only depends on the illuminant and its reflectance. For example, the observed spectrum of an ordinary reflective surface with reflectance R and illuminant I is

$$P(\lambda) = I(\lambda)R(\lambda),$$

where $I(\lambda)$ is the intensity of the illuminant at wavelength λ and $R(\lambda)$ is the reflectance of the material at wavelength λ . If we capture the object with a charge-coupled device (CCD) camera from three channels R, G and B, the color of each pixel for each channel is

$$p = \int \bar{c}(\lambda)I(\lambda)R(\lambda)d\lambda, \quad (3.1)$$

integrated over visible spectrum (380 nm to 720 nm), where $\bar{c}(\lambda) = \{\bar{r}(\lambda), \bar{g}(\lambda), \bar{b}(\lambda)\}$ are the camera response curves for each channel [43].

However, for a pure fluorescent material, the observed spectrum depends on the illuminant, the material's Excitation spectrum and Emission spectrum. For each wavelength in an Excitation spectrum, there is a corresponding Emission spectrum that shows the frequency distribution and intensity of the emitted light. Suppose the illuminant I and its intensity at wavelength λ_i is $I(\lambda_i)$. Let Ex and Em represent the normalized excitation and emission spectrum respectively ¹. Considering the sum of the contribution from illuminant, excitation and emission, the observed spectrum at λ_i can be expressed as

$$P(\lambda, \lambda_i) = I(\lambda_i)Ex'(\lambda_i)Em(\lambda)d\lambda, \quad (3.2)$$

where $Ex'(\lambda_i) = \frac{Ex(\lambda_i)}{\int Ex(\lambda_i)d\lambda_i}$ is the relative intensity of the excitation caused by illuminant at wavelength λ_i . [44]. By summing up $P(\lambda, \lambda_i)$ for all wavelength λ_i , we can get

$$P(\lambda) = \left(\int I(\lambda_i)Ex'(\lambda_i)d\lambda_i \right) Em(\lambda), \quad (3.3)$$

If we capture the pure fluorescent material with a CCD camera, the color of the pixel for each channel can be expressed as

$$p = \left(\int I(\lambda_i)Ex'(\lambda_i)d\lambda_i \right) \int \bar{c}(\lambda)Em(\lambda)d\lambda, \quad (3.4)$$

Because of these properties, as a common phenomenon, fluorescence motivates people to develop a new method for measuring food quality if there are fluorescent components that are relevant to quality in food.

¹Both Excitation spectrum and Emission spectrum are normalized so that the minimum intensity is 0 and the maximum intensity is 1.0.

3.2 Fluorophores in Food

As introduced in the previous section, fluorescence is a unique spectroscopic technique because of inherently properties. Every kind of fluorophore needs the energy of a specific level to be excited and fluoresce. All fluorophores have independent spectral excitation and emission profiles that correspond to their unique fluorescent properties, and can be measured as excitation-emission spectra or excitation-emission matrix (EEM). Besides, the Stoke shift property of fluorescence also makes it a very sensitive analytical method for all kinds of measurement.

However, if we want to measure food quality through fluorescence, the precondition is that we are clear about whether food contains fluorescent component, and which kind of component food contains. People have found the appearance of fluorescence on many kinds food such as banana a long time ago (Figure 3.3) [7, 45]. Scientific research shows that food contains abundant species of natural fluorescent compounds which are important for nutrition and taste. Such kind of fluorescent chemical components are usually called fluorophore and can be divided into two main classes intrinsic and extrinsic [46]. Intrinsic fluorophores are those that occur naturally. Extrinsic fluorophores are those that are added to the sample to provide fluorescence when none exists. Generally speaking, intrinsic fluorophores are used for measurements. Intrinsic fluorophores include the aromatic amino acids, NADH, flavins, chlorophyll and so on.

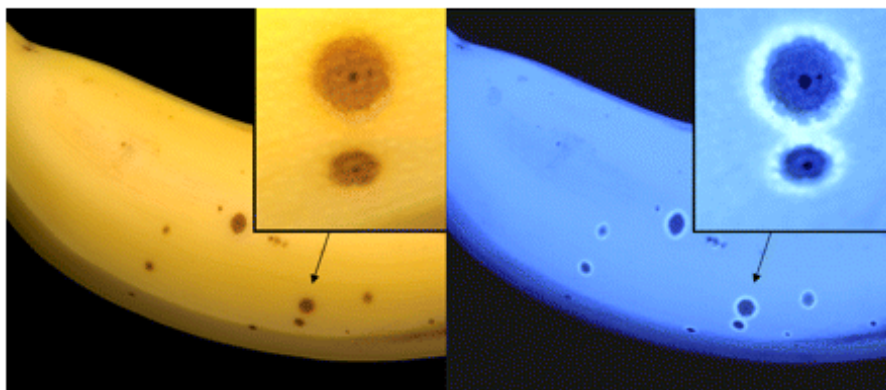


Figure 3.3: The fluorescence on the surface of banana [7].

One of the earliest reviews on naturally occurring fluorophores was written by Wolfbeis in 1985 [47]. This review included several food-relevant fluorescent compounds such as aromatic amino acids, vitamins, flavonoids and so on. In 2005, a Web-based food fluorescence library was made available at www.models.kvl.dk (September 2005) with the fluorescence characteristics of a variety of intact food samples as well as a list of food-relevant single fluorophores [48]. Eleven kinds of primary fluorophores and 27 intact food samples are measured in all. The fluorescence spectral parameters of these selected fluorophores are presented in Table 3.1. The EE spectra and EE matrix of these fluorophores are shown in Figure 3.4 and 3.5¹ [49].

Table 3.1: List of 11 food-relevant fluorophores and their fluorescent properties. (Data from the food fluorescence database at www.models.kvl.dk.)

NO.	Fluorophore	Excitation λ_{max} (nm)	Emission λ_{max} (nm)
1	Phenylalanine	258	284
2	Tyrosine	276	302
3	Tryptophan	280	357
4	Vitamin A (retinol)	346	480
5	Vitamin B ₂ (riboflavin)	270 (382, 448)	518
6	Vitamin B ₆ (pyridoxin)	328	393
7	Vitamin E (α -tocopherol)	298	326
8	NADH	344	465
9	ATP	292	388
10	Chlorophyll A	428	663
11	Hematoporphyrin	396	614

¹The shown EE data are all measured on Perkin Elmer LS50 B spectrofluorometer. The fluorescence database also provides the data measured on Varian Cary Eclipse spectrofluorometer. For more details, please refer to the website: www.models.kvl.dk.

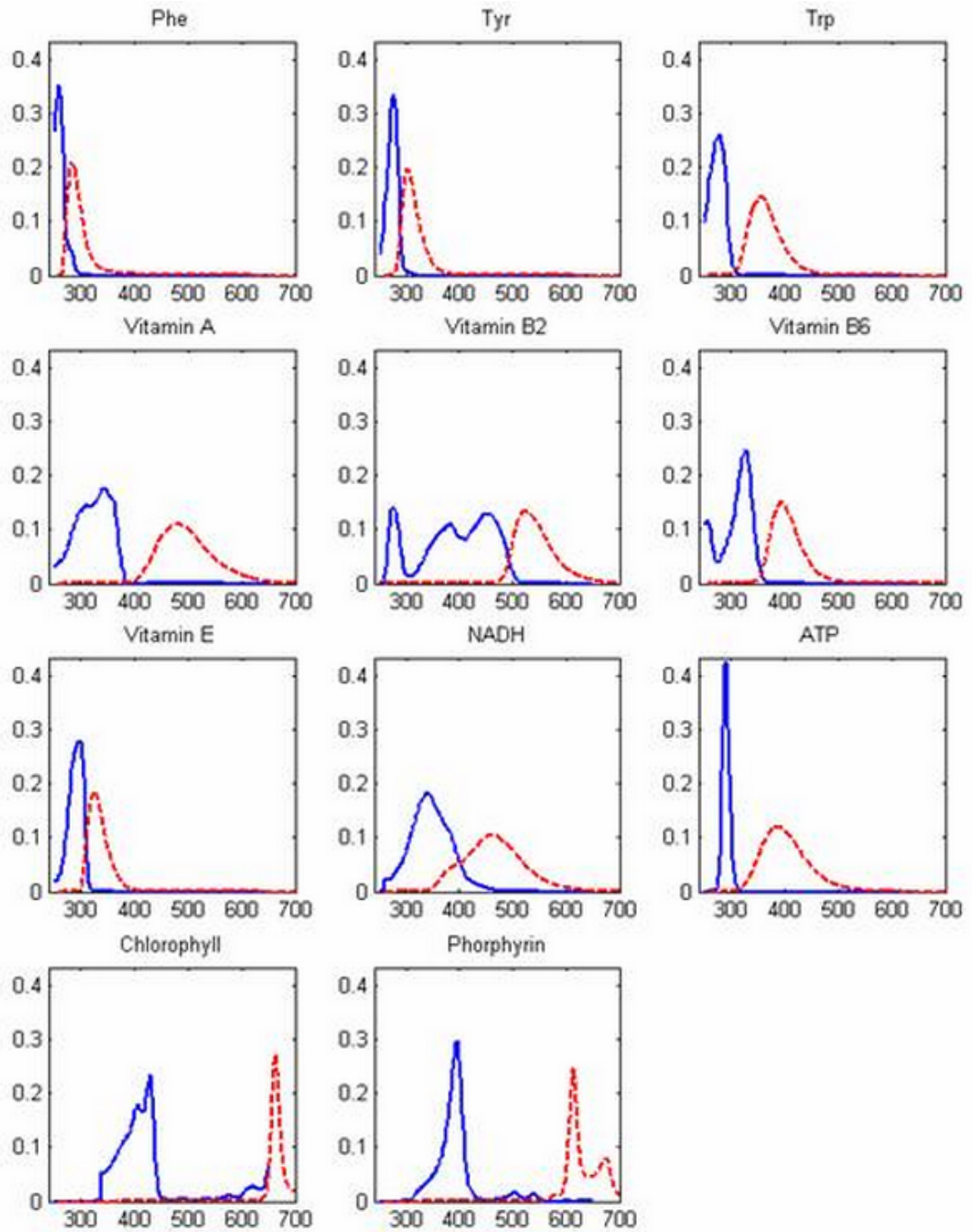


Figure 3.4: Excitation and emission spectra of the 11 fluorophores.

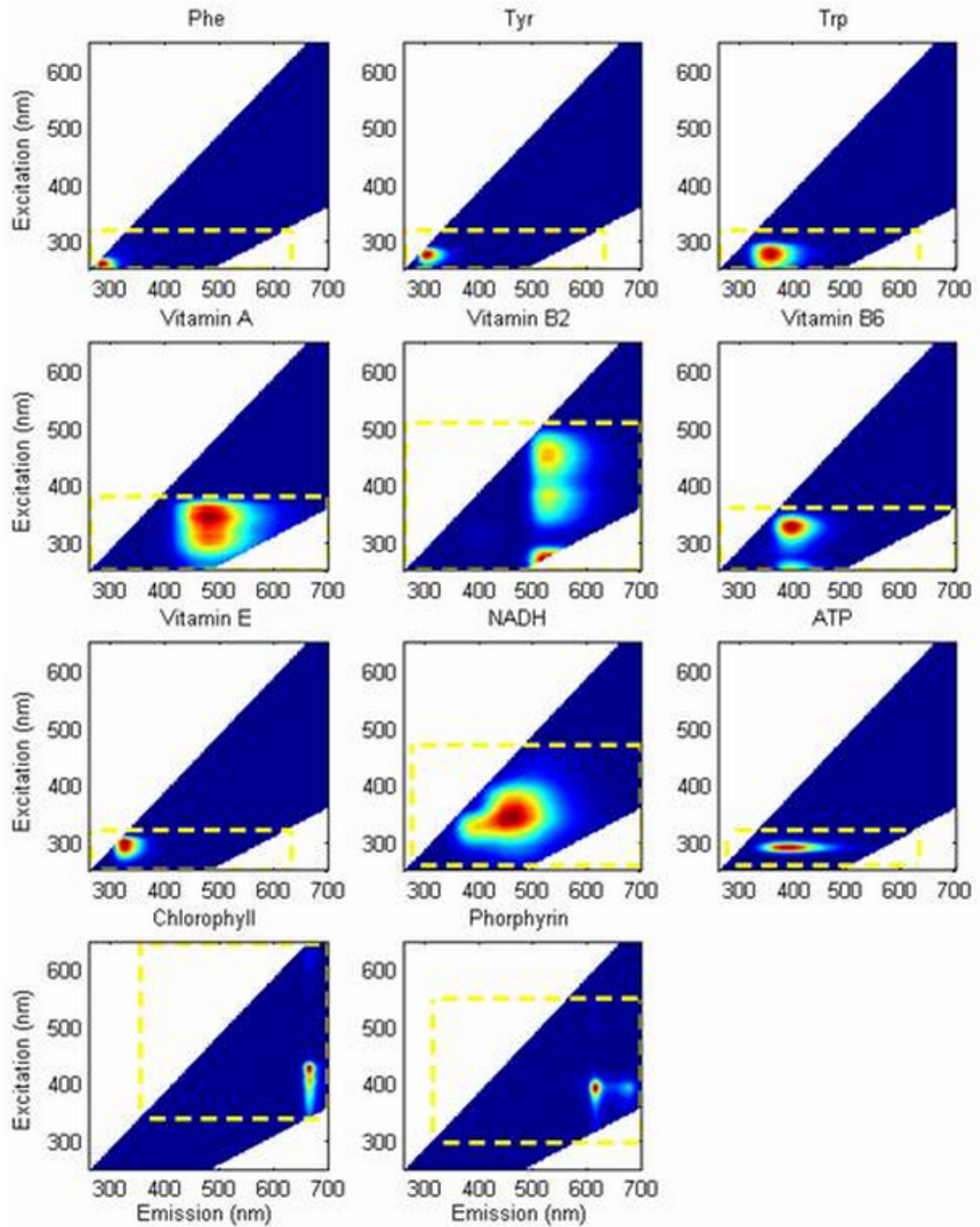


Figure 3.5: Excitation-Emission Matrix of the 11 fluorophores.

3.3 Fluorescence and Food Quality

In the previous section, we introduced 11 primary fluorophores in food. In general, one kind of food contains not only one kind of fluorophore. The fluorescence we catch from food under an excitation wavelength is always a superposition of the fluorescence emitted from a few fluorophores. These superposition of fluorescence is found to be highly related to food quality. A simple example is that since food quality changes after being cooked, we can clearly observe that from the Excitation-Emission spectra (Figure 3.6 [50]). For some kinds of food, quality is evaluated through the content of specified components, such as the ratio of buckwheat flour in dried buckwheat noodles. For some other kinds of food, the quality can be evaluated with many indicators, such as meat. We can simply divide meat into fresh meat and spoiled meat. As to fresh meat, people also use tenderness, palatability and many indicators to evaluate its quality. In the case of spoiled meat, the spoilage of meat is a very complex physical and chemical process. Some fluorescent components decompose while other fluorescent components generate. As a result, the fluorescence observed from meat changes constantly. Next, we take meat for example to talk about some previous work which correlated fluorescence with meat quality and spoilage.

On the whole, the measurements of fluorescence from collagen, elastin, adipose tissues, and protein are widely used to estimate meat quality [51, 52]. These components are thought to be an important parameter of meat quality. More accurately speaking, the fluorescence is basically contributed by 4 kinds of fluorophores. They are tryptophan, NADH, tyrosine and riboflavin, whose EE spectra are shown in Figure 3.7 and 3.8 [53].

Since 1987 Swatland has written a series of papers on different aspects of the autofluorescence of meat [54]. He caught the collagen and elastin fluorescence from meat using excitation at 365 nm. The obtained fluorescence were correlated to several sensory-related quality parameters such as gristle content in beef, skin content of poultry meat slurry [55], and turkey meat [56], palatability [57], chewiness [58], and toughness [59] of beef. All these correlations can be considered as indirect analyses due to the fact that these quality parameters are related to the amount and distribution of connective and adipose tissue in the meat. By using excitation wavelengths between 332 and 380 nm, Hildrum *et al.* successfully use FFFS to estimate the tenderness of muscles [60]. Besides, in some other work, fluorescence emission spectra of various types of collagen in meat products were

found to correlate with tensile properties [61], water-holding capacity [62], and so on.

Moreover, tryptophan has been correlated to the texture of meat emulsions, sausages [63, 64], and meat tenderness [52]. Frencia *et al.* use FFS method to discriminate five kinds of muscle that present different levels of collagen contents at two time points (2 and 14 days post mortem). By applying FDA to the tryptophan fluorescence spectra, they obtained the correct classification rate of 82%. This method shows that the front-face spectra of tryptophan is useful to identify the maturation degree of meat.

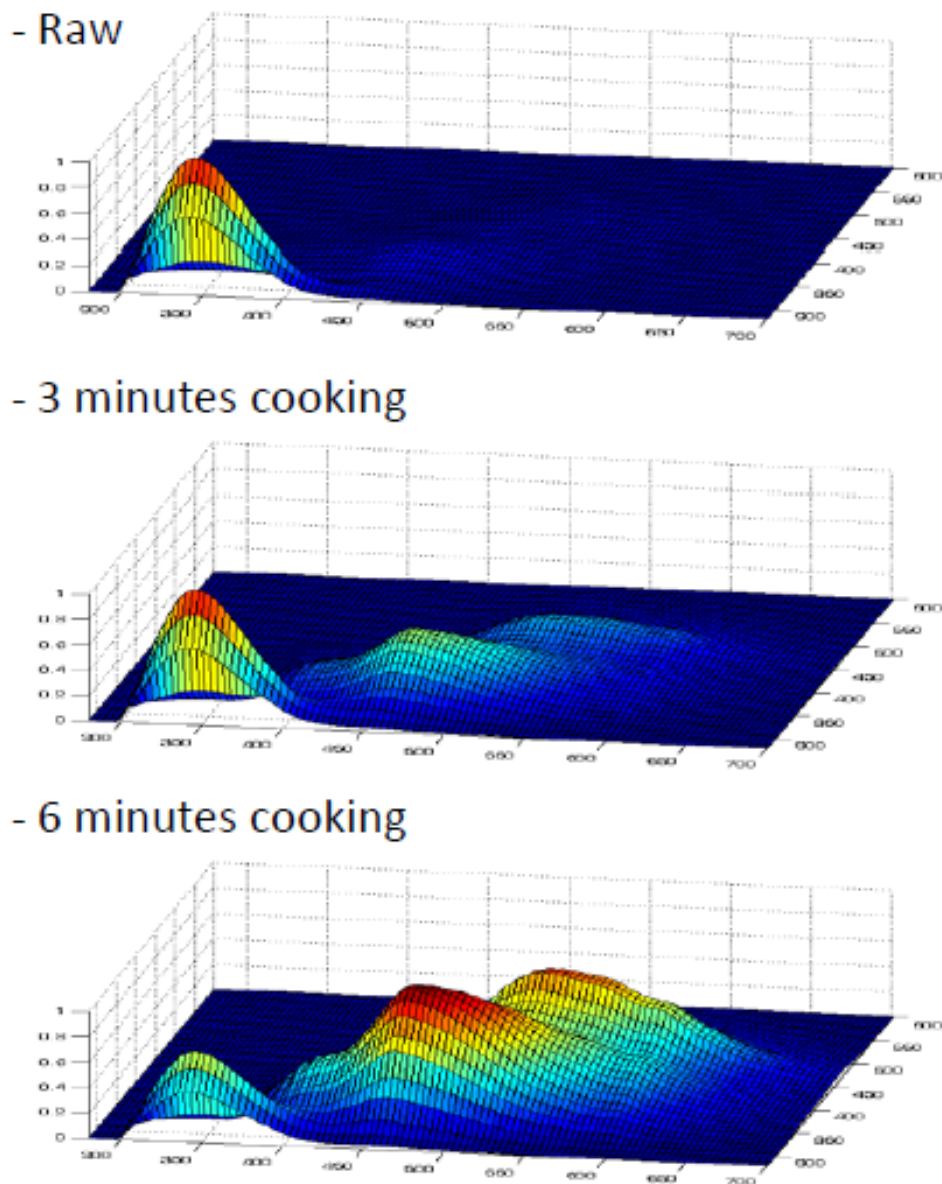


Figure 3.6: EE spectra changes as meat being cooked.

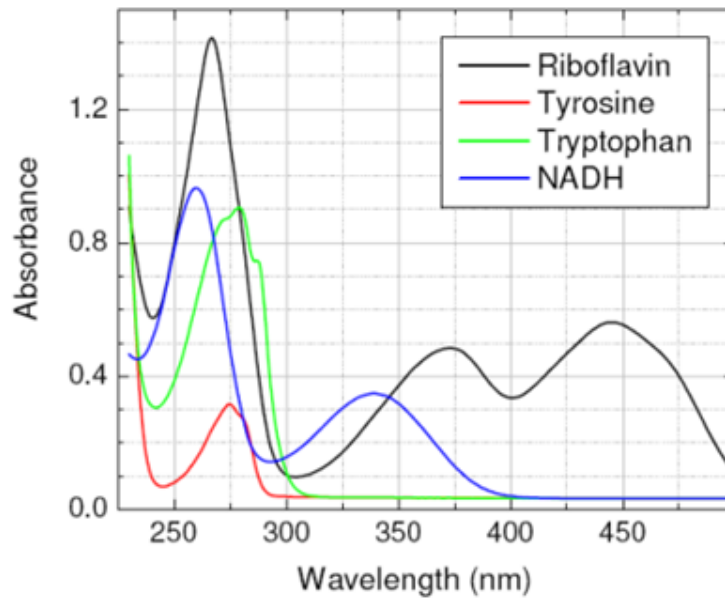


Figure 3.7: Excitation spectra of 4 primary fluorophores in meat.

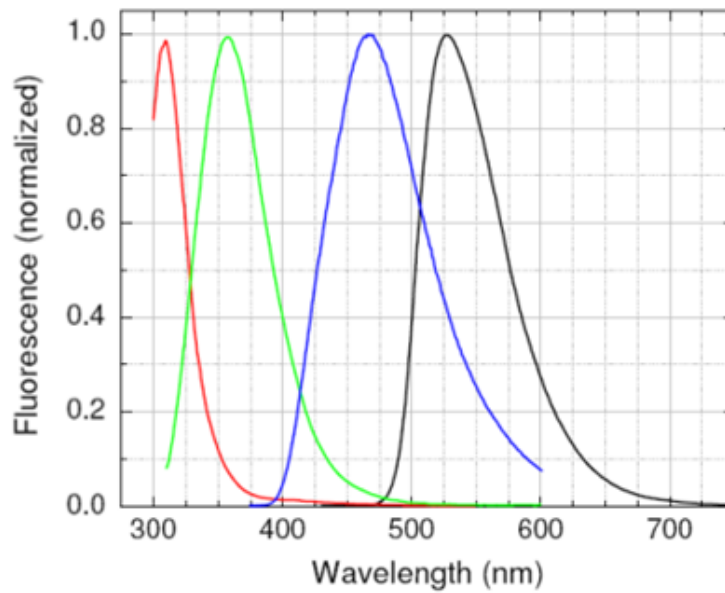


Figure 3.8: Emission spectra of 4 primary fluorophores in meat.

Further more, lipid oxidation is thought to be another important factor that limits the quality and acceptability of meat and meat products [65]. Fluorescence emission spectra from fluorescent oxidation products have been found to correlate with lipid oxidation [66] and rancidity [67] of meat.

On the other hand, meat is susceptible to spoilage caused by physical damage, chemical changes and microbial spoilage. Among this three ways, microbial spoilage is the most significant to cause meat deterioration. On the other hand, a lot of components of bacteria such as proteins and vitamins are fluorescent which make fluorescence spectroscopy a valuable technique for the determination of microbial spoilage in meat. In another work, the change of fluorescence on the surface of pork with time is explained by degradation of the tryptophan in pork meat caused by the growing bacteria [68]. Specifically, there were two kinds of tryptophan on meat surface. One was from pork meat and another one was from microorganisms. The fluorescence intensity decreased with time because the decrease in tryptophan from pork meat outweighed the increase in tryptophan from microorganisms. Therefore it could be said that there is a high correlation between fluorescence and the spoilage of meat (Figure 3.9).

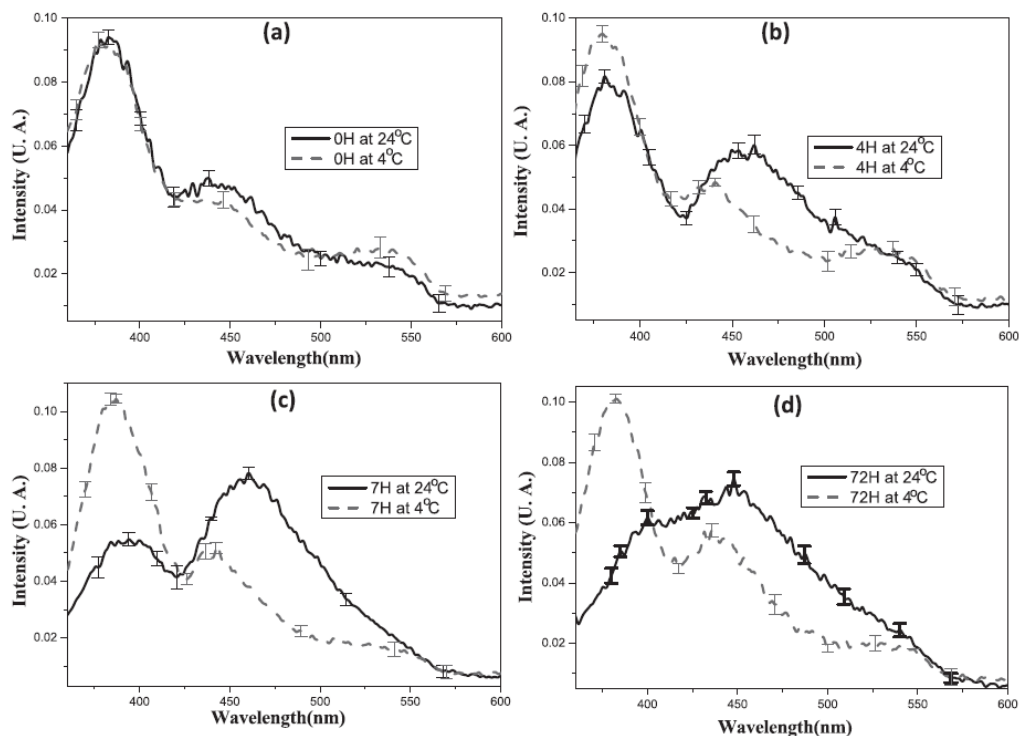


Figure 3.9: Fluorescence spectra of pork meat stored under different temperature measured at different storage times.

Chapter 4

Proposed Method

As introduced in the previous chapter, fluorescence is highly correlated to food quality. So we proposed a new method to measure food quality by using fluorescence images. We first did experiment on meat, and presented a method to catch the fluorescence of meat as image in the middle range of visible wavelength. After that, due to the qualities of meat are too complex, we shifted experiment materials to buckwheat noodles whose quality is simply determined by buckwheat flour ratio. Estimating buckwheat flour ratio is the most suitable case to be used to prove our method is feasible.

4.1 The Model of Reflective and Fluorescent Components in an Image

Equation 3.4 has shown us the pixel for each channel when we take photos of a pure fluorescent material by a CCD camera. When we take an image of composite objects with both ordinary reflective and fluorescent components using a CCD camera, the color of each pixel p can be represented as follow [44]:

$$p = \int \bar{c}(\lambda)I(\lambda)R(\lambda)d\lambda + \left(\int I(\lambda_i)Ex'(\lambda_i)d\lambda_i \right) \int \bar{c}(\lambda)Em(\lambda)d\lambda, \quad (4.1)$$

This means each pixel p in the final image for each channel R, G, B is just the sum of the pixel of reflective components and fluorescent components. This linear model made it possible for us to get fluorescence images easily by doing difference of images.

4.2 Observation of Fluorescence

Meat

After surveying on the primary fluorophores in pork meat, we finally focused on NADH in meat though some previous work about pork fluorescence mainly talked about tryptophan. Both meat and bacteria on the surface of meat contains NADH. As meat goes bad, the NADH of meat decomposes while the NADH in bacteria increases with a faster speed. So we expected to find some important changes from the fluorescence image of NADH.

Considering the excitation spectrum of NADH, we chose a 370 nm UV light as light source. We take two pieces of photos of the board from the same direction, same distance, in the same environment. One is taken under ambient light, the other is taken after adding UV light to the environment. Then we compute the difference of these two images on R, G and B channel, and name the result channels as FR, FG and FB channel respectively. Thus the components of UV light and emitted fluorescence from eat should be recorded in these 3 new channels. Since the emission peak of NADH is around 470nm, fluorescence should be responded better in FG and FB channel. Moreover, considering FB channel has a strong response to blue light, we finally focus on FG channel. The photographic method and principle of catching fluorescence are shown in Figure 4.1.

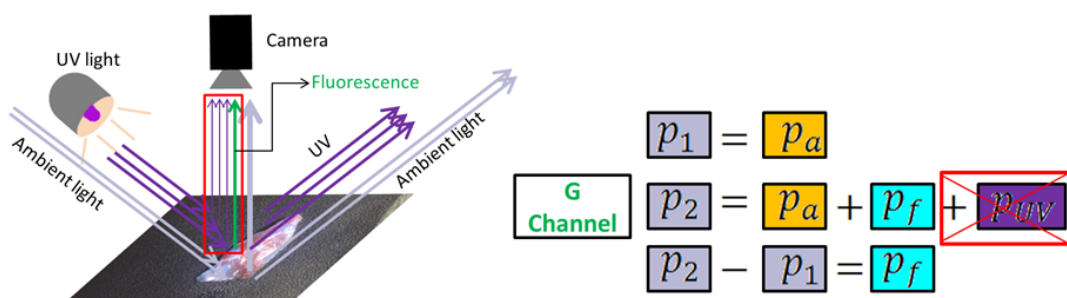


Figure 4.1: Photographic method and principle of catching fluorescence. In the formula, p_a represents the image taken only under ambient light. p_f represents the image of fluorescence component. p_{uv} represents the image of UV component.

Buckwheat Flour

Figure 4.2 shows us the EEM of buckwheat flour and wheat flour [21]. We can see their emission spectra are nearly the same besides the red circled area. Considering this

delicate difference, we use 650 nm band-pass filter before camera to get the fluorescence information at 650nm only. Then we use another filter in front of light source to cut all the light whose wavelength is more than 400 nm. We expected to use this simple method to observe buckwheat fluorescence in commercial buckwheat foods.

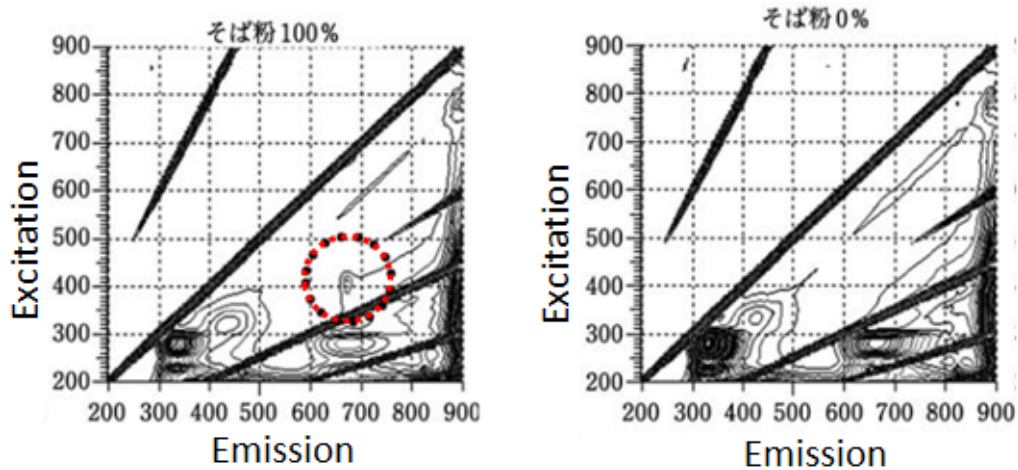


Figure 4.2: EEM of buckwheat flour (left) and wheat flour (right).

4.3 Estimation of Buckwheat Flour

Overview of Proposed Method

Comparing the EEM of buckwheat and wheat flour in Figure 4.2, we still used 370 nm UV light as excitation light while chose 6 wavelengths to take photos this time. We used 420 nm, 450 nm, 532 nm, 580 nm, 610 nm and 650 nm band-pass filters to realize this. By using the photographic method mentioned in Figure 4.1, we got two series of images for each mixed flour sample at each wavelength, one series is taken under ambient light, the other series is taken under ambient light plus UV. Each series of images include 20 pieces of images for denoising. After data collection, we continued as following steps:

(1) Calculate relative pixel value by using following equation:

$$I = \frac{I_0 - B}{W - B} \quad , \quad (4.2)$$

Chapter 4 Proposed Method

where where I was the relative-reflectance of an image; I_0 was the original image; B was the dark image, and W was the white image.

- (2) Then chose to use the FB channel images for 420 nm and 450 nm, FG channel images for 532 nm and 580 nm, FR channel images for 610 nm and 650 nm separately to extract image features.
- (3) Locating the center of fluorescence images, define a circular region whose radius is 100 pixels. For the 6 fluorescence images of each powder sample, the position of this region is ensured to be identical.
- (4) For each sample, compute average pixel value of selected region from 6 fluorescence images as: $x_1, x_2, x_3, x_4, x_5, x_6$. Buckwheat ratios of these samples are known as y in advance.
- (5) Build prediction model by using partial least squares regression (PLSR).

The whole process is shown in Figure 4.3.

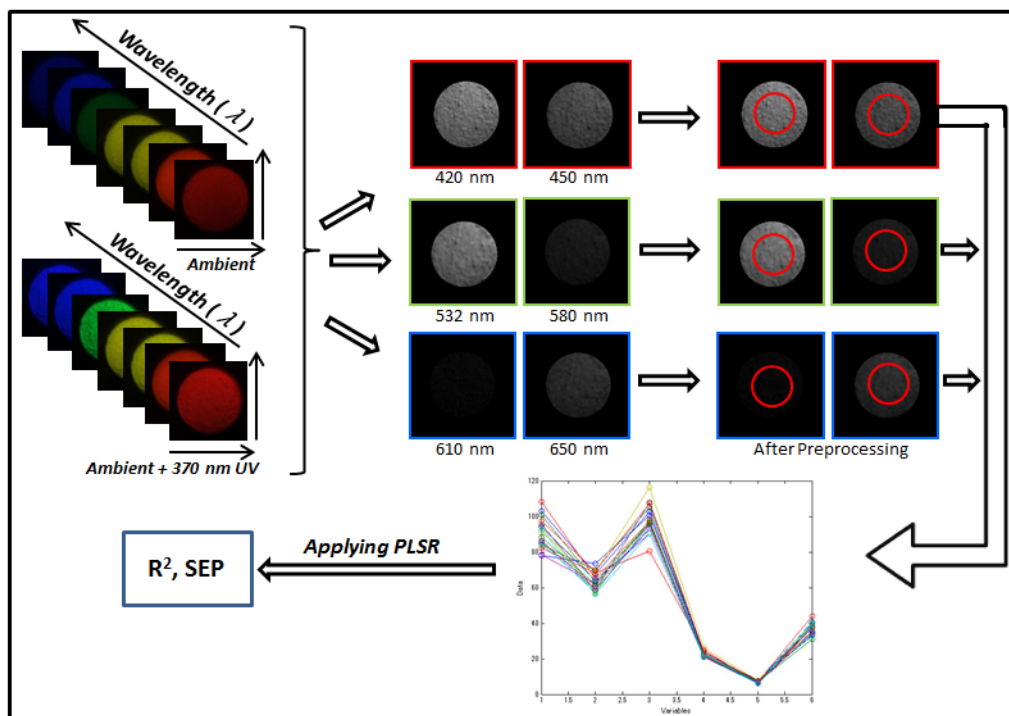


Figure 4.3: Schematic flow of the proposed method.

The Use of PLSR

PLSR was applied to the average pixel data of the calibration datasets by setting real buckwheat ratios as responses to build model, and predict the buckwheat flour ratio of validation datasets. In this thesis, the number of latent variables was determined when RMSEP is the lowest and predictor variables are as few as possible. The performance of prediction model was finally evaluated by the coefficient of determination (R^2) and standard error of prediction (SEP).

SEP is defined as below:

$$RMSEP = \sqrt{\frac{PRESS}{n}} = \sqrt{\frac{\sum (y_i - \hat{y}_i)^2}{n}}, \quad (4.3)$$

where y_i represents true value while \hat{y}_i represents the prediction value.

R^2 is defined as below:

$$R^2 = 1 - \frac{\sum (y_i - f_i)^2}{\sum (y_i - \bar{y})^2}, \quad (4.4)$$

where y_i is called the observed value and f_i is sometimes called the predicted values; \bar{y} is the mean of observed data.

Removing Influence of Shadows

Due to the surface of powder samples are not so flat, there are many shadows in final fluorescence images. These shadows have strong impact on the mean pixel value of selected regions, which influence the predicting result. Only computing the pixels of top 20, 50 or 100 brightness in the selected region can remove this influence in theory. The result of our experiment shows that using top 50 brightness can obtain best effect.

Chapter 5

Experiments

5.1 Materials

In the first experiment, we tried to observe fluorescence changes as meat goes bad. Pork loin pieces bought from supermarket in the morning were used. The pork was ensured to have abundant lean, fat and marble on the surface. To avoid bringing in extra bacteria from knife, the pork was kept its original shape without any cutting. The pork was stored at room temperature with a glass cover on it so that the water in the meat doesn't evaporate. Besides, we continuously kept the meat for 7 days without letting anything come into contact with its surface to get samples of different freshness.



Figure 5.1: 4 kinds of materials.

In the second experiment, we tried to estimate the ratio of buckwheat in a mixed powder of buckwheat and wheat flours. Common pure wheat flour (AEON Corp.) and buckwheat flour (Masudaya Food Corp.) bought from supermarket was used. The flours were ensured to contain 100% buckwheat (or wheat flour). Besides, we tried to make the flours do not include any additional ingredients such as egg, milk, shrimp, and so on. By using these two pure flours, we prepared mixed powder in which buckwheat flour ratio ranged from 0% to 100% at 20% interval. After making up, we repeatedly put some powder in a 20mm diameter dish and take images from 6 wavebands. For each ratio, we prepared 4 different samples to take images, thus we finally collected data from 24 samples.

In the last experiment, we tried to observe fluorescence of buckwheat at 650 nm from both dried and boiled buckwheat noodles. Five products of commercially available dried noodles were used. Three of them were dried buckwheat noodles whose buckwheat ratio separately was 100%, 80% and 50%. The left two products were Udon and Pasta in which buckwheat ratio is 0%. Details on the ratio of the buckwheat flour in these samples were provided by manufacturers. All the materials are shown in Figure 5.1.

5.2 Image Acquisition and Preprocessing

Figure 5.2 shows the imaging system used in our experiments. This imaging system composed of a camera, two illuminants and a filter wheel with 6 band-pass filters attached to it. The camera we used is Chameleon CMLN-13S2C camera, which is a normal colorful CCD camera. Band-pass filters used are of narrowband range with center wavelength at 420nm, 450nm, 532nm, 580nm, 610nm, and 650nm respectively. To do a contrast experiment, we use two light sources: a 370 nm UV light and a common blue light. To ensure the imaging system collect effective data, we make sure the settings of camera and light are the same when we took images at a specific wavelength.

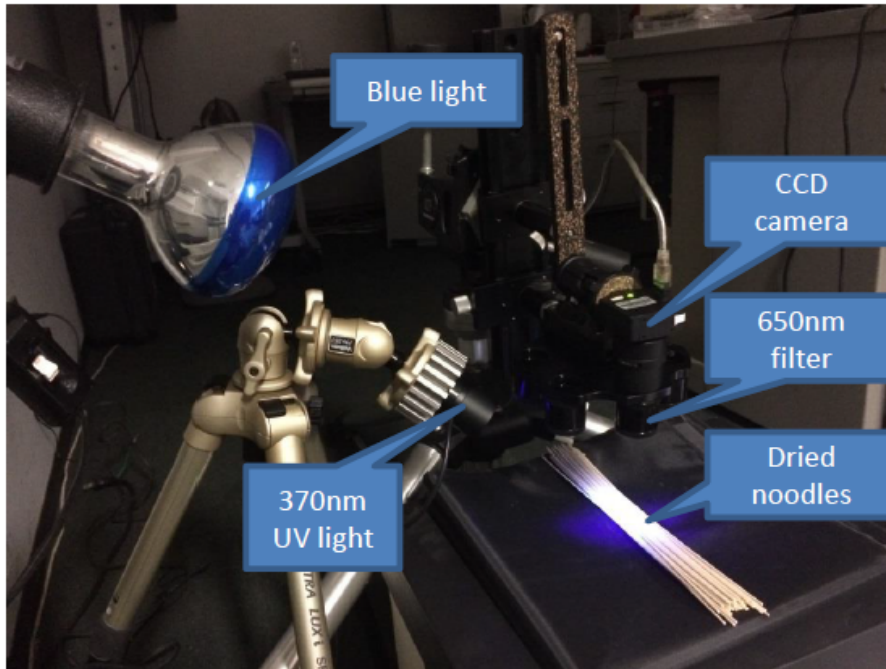


Figure 5.2: The imaging system in our experiments.

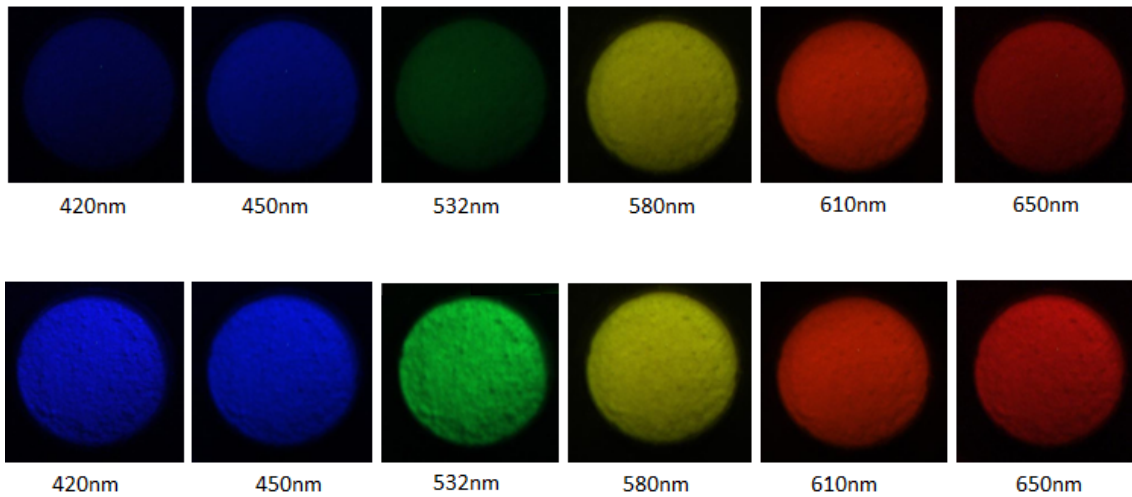


Figure 5.3: Example of 6 spectral images of a flour sample after preprocessing. Upper row of images were taken under ambient light. Lower row was taken under ambient plus 370 nm UV light.

5.3 Estimation of Buckwheat Flour Ratio

In this experiment, we totally prepared 24 mixed powder samples, and extract data through computing mean pixel value of ROI in relevant channels (FR, FG or FB). Thus each sample has six features ($x_1, x_2, x_3, x_4, x_5, x_6$), which separately represents the pixel value computed at 6 wavelengths. The buckwheat flour ratio in the sample is defined as y . We divided the 24 samples into 4 sets, then used 3 of them (18 samples) for calibration and the 4th set (6 samples) for validation. PLS regression model was built by using leave one out cross validation on calibration data set. Then the validation set was used to assess the prediction model. The relationship between SEP and number of latent variables is shown in Figure 5.4.

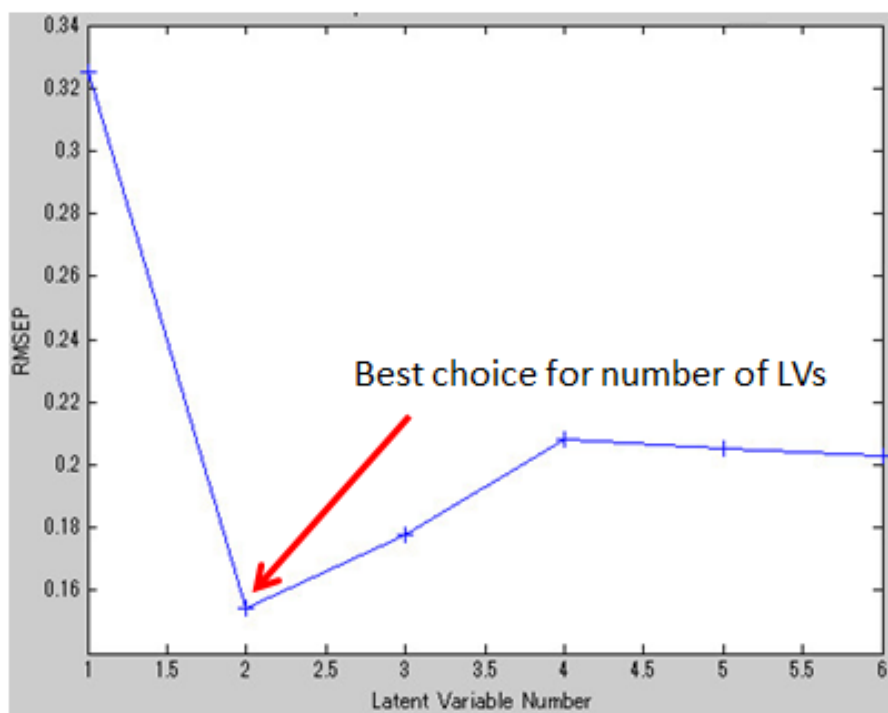


Figure 5.4: Changes of SEP with the number of latent variables.

We can see, the least standard error of prediction can be got when two latent variables are used to build model. In this situation, the relationship between the true and predicted buckwheat flour ratios of calibration and validation datasets are shown in Figure 5.5.

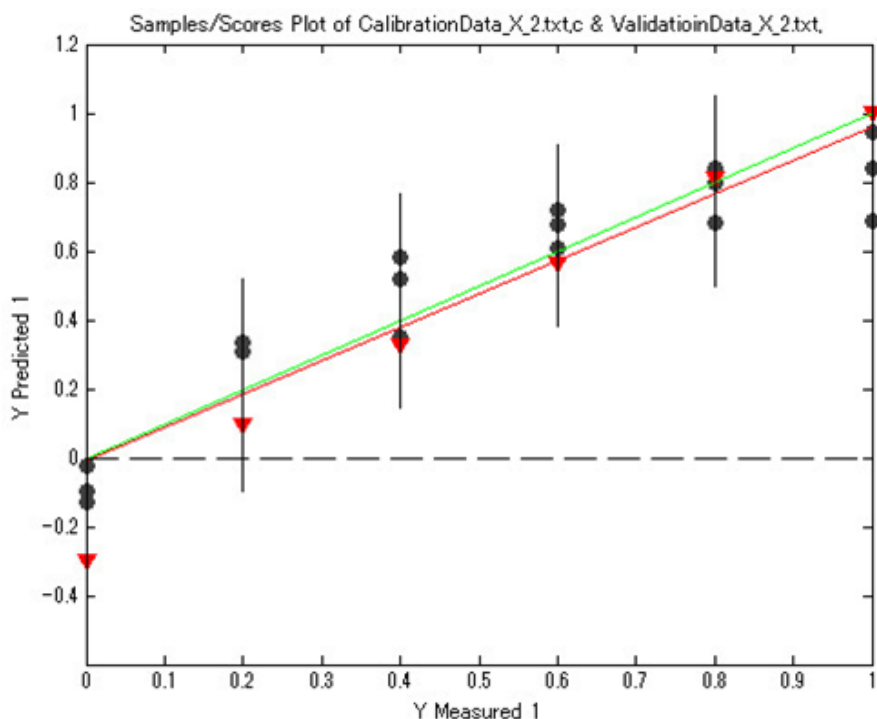


Figure 5.5: Relationship between true and predicted buckwheat flour ratios. Black spots represent calibration set, while red triangle represent validation set.

Then we chose 3 sets for calibration and the left one set for validation in turn, and did a statistics on the mean absolute error, standard error and R^2 of prediction. Table 5.1 shows the statistical result.

Table 5.1: Statistics of the prediction result of 4 dataset combinations.

True ratio	0.00	0.20	0.40	0.60	0.80	1.00	Mean	Pred R^2
Pred1	-0.36020	0.09357	0.31813	0.56140	0.81404	1.0058	0.0411	0.986679
Pred2	-0.09303	0.58553	0.38553	0.60658	0.68289	0.80921	0.1191	0.743245
Pred3	0.079245	0.37183	0.41743	0.66822	0.9684	0.92281	0.0971	0.938874
Pred4	-0.18977	0.26053	0.48567	0.72251	0.66988	0.66966	0.1215	0.74514
Mean	0.1805	0.1811	0.0499	0.0590	0.1074	0.1509	0.0947	0.8535

From table 5.1, we can see the mean prediction error of model is no more than 0.1. It means that the model acceptable even though we haven't removed the influence of shadows on the surface of samples yet. A comparison between previous method [21] and our method is shown in table 5.2.

Table 5.2: Comparison of previous and our method.

	Cal R^2	Pred R^2	SEC	SEP
Previous method	0.999	0.988	0.00426	0.03487
Our method	0.863694	0.986679	0.126104	0.131205

After that, we computed the average pixel value of all the pixels of top 50 brightness in the image in order to remove the influence of surface shadows. At the same time, we also used multiple linear regression (MLR) to build prediction model. By using two groups of datasets for calibration and validation, we did a comparison between MLR and PLSR. A statistics of comparison result is shown in table 5.3 and 5.4.

Table 5.3: Comparison result on data group 1.

True	0.00	0.20	0.40	0.60	0.80	1.00	Mean	Pred R^2	SEP
PLS	-0.19396	0.26053	0.4038	0.54708	0.73947	0.95643	0.0369	0.953489	0.0921618
MLR	-0.18567	0.24825	0.39971	0.54298	0.73129	0.96053	0.0356	0.959619	0.0891133

Table 5.4: Comparison result on data group 2.

True	0.00	0.20	0.40	0.60	0.80	1.00	Mean	Pred R^2	SEP
PLS	0.04238	0.51433	0.55526	0.65351	0.77222	1.0137	0.0941	0.861838	0.15075
MLR	0.04795	0.46199	0.68655	0.81754	1.0842	1.3275	0.2296	0.959799	0.261743

From above two tables, we can see MLR has a better R^2 but a poorer SEP than PLSR, which means model built by MLR has a better fitting effect, but a large prediction error. Besides, the decrease in mean absolute errors shows that removing pixels in shadow areas improved the performance of prediction model.

5.4 Observation of Fluorescence

Meat

We kept taking photos of a same piece of meat once a day for four days, until we can judge its spoilage on sensory. Figure 5.6 shows the FG channel images of each day. From

this figure, we can clearly see that the intensity of fluorescence increased as meat went bad. This is a little different from the result of Nishino-san's work [41]. We suspect that this is because we aimed at different fluorophores in meat. Their method focused on tryptophan while our method focused on NADH. Since obvious fluorescence changes were observed as meat went bad, it is feasible to estimate meat qualities like freshness through fluorescence images.

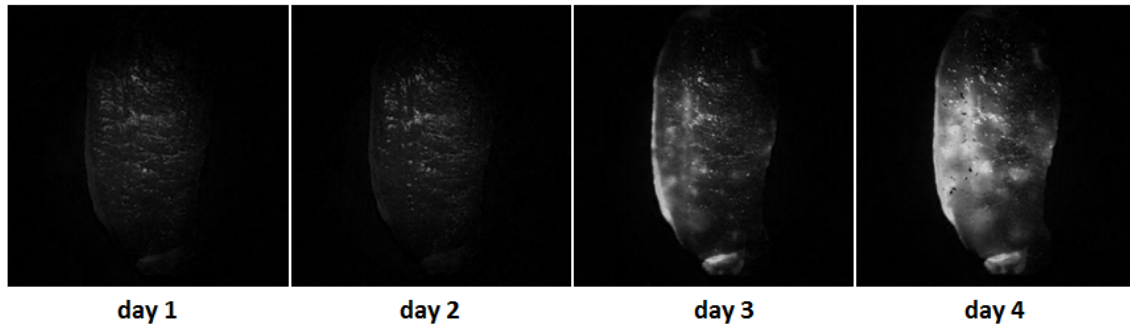


Figure 5.6: Fluorescence images of pork meat.

Buckwheat Noodles

We used another ordinary blue light besides 370 nm UV light as light source to do the experiment. All the images were taken at 650 nm by using a band-pass filter in front of CCD camera. Either 370 nm UV light or blue light was turned on during each shot. We first did experiment on dried noodles of 0%, 50%, 80% and 100% buckwheat. Then we did the same experiment on boiled samples. The results are shown in Figure 5.7 and Figure 5.8. Comparisons of the fluorescence images taken under two light sources are shown in Figure 5.9 and Figure 5.10. From Figure 5.9, we can see, from left to right, as buckwheat ratio decreases, the fluorescence images taken under UV light became darker while images taken under blue light became brighter. We can observe the same result from Figure 5.10. This is actually caused by reflected light. The UV light source centers on 370 nm, while the blue light has a much wider spectral range. As buckwheat ratio decreases, the color of noodle samples change from dark to bright color, which makes their surface reflect more light from blue light. As a result, from 100% buckwheat to udon, fluorescence images taken under blue light became brighter and brighter. This contrast experiment shows that the fluorescence of buckwheat can be observed at 650 nm as long as we removed reflected light. We expect this method to be a revolutionary nondestructive technique to visualize buckwheat content in all kinds of commercial buckwheat products.

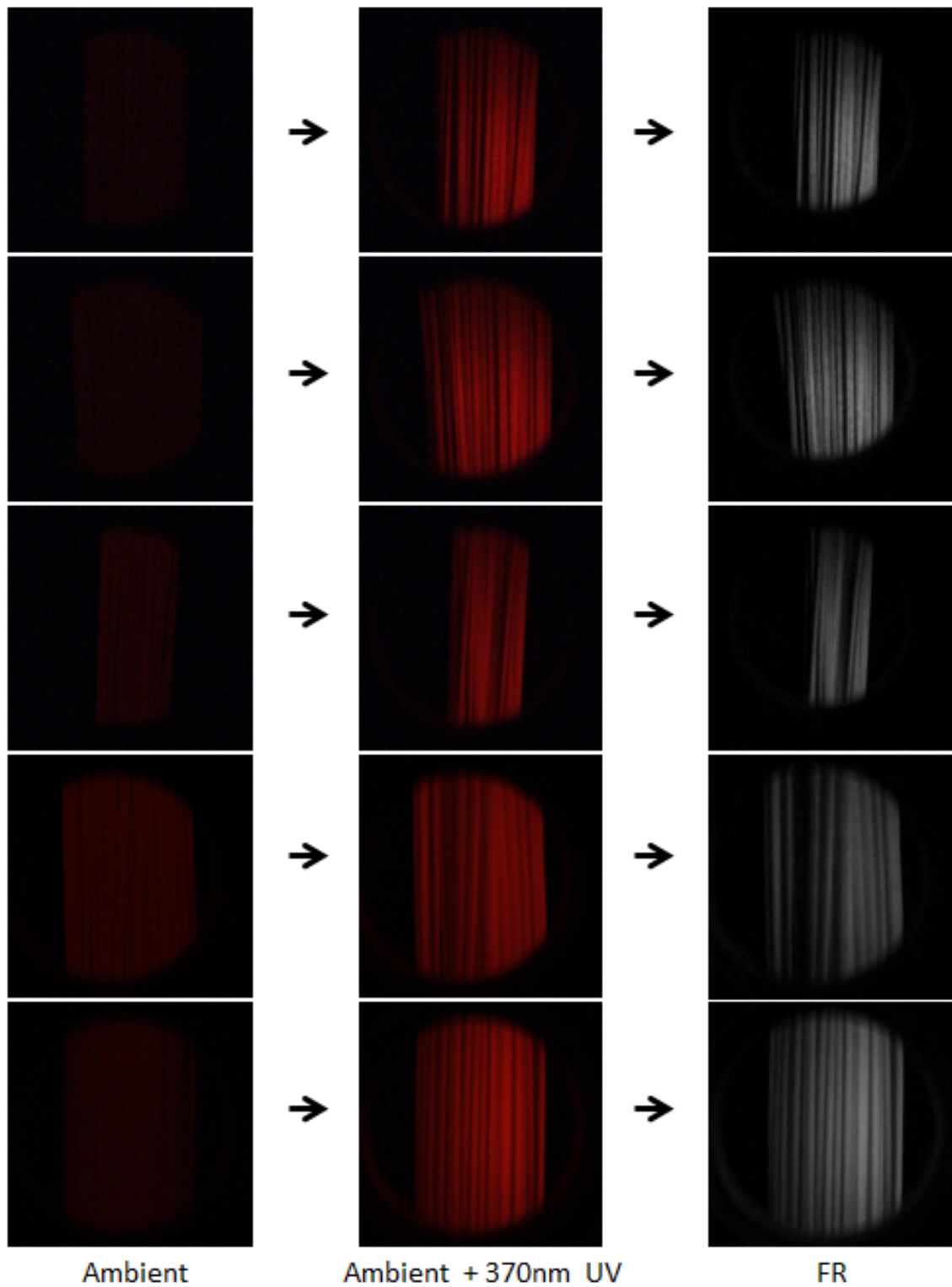


Figure 5.7: Images of dried noodles taken at 650nm. From top to bottom: 100% buckwheat noodle, 80% buckwheat noodle, 50% buckwheat noodle, Udon and Pasta. Images in the left column were taken under ambient light, while the middle column were taken under ambient and UV light.

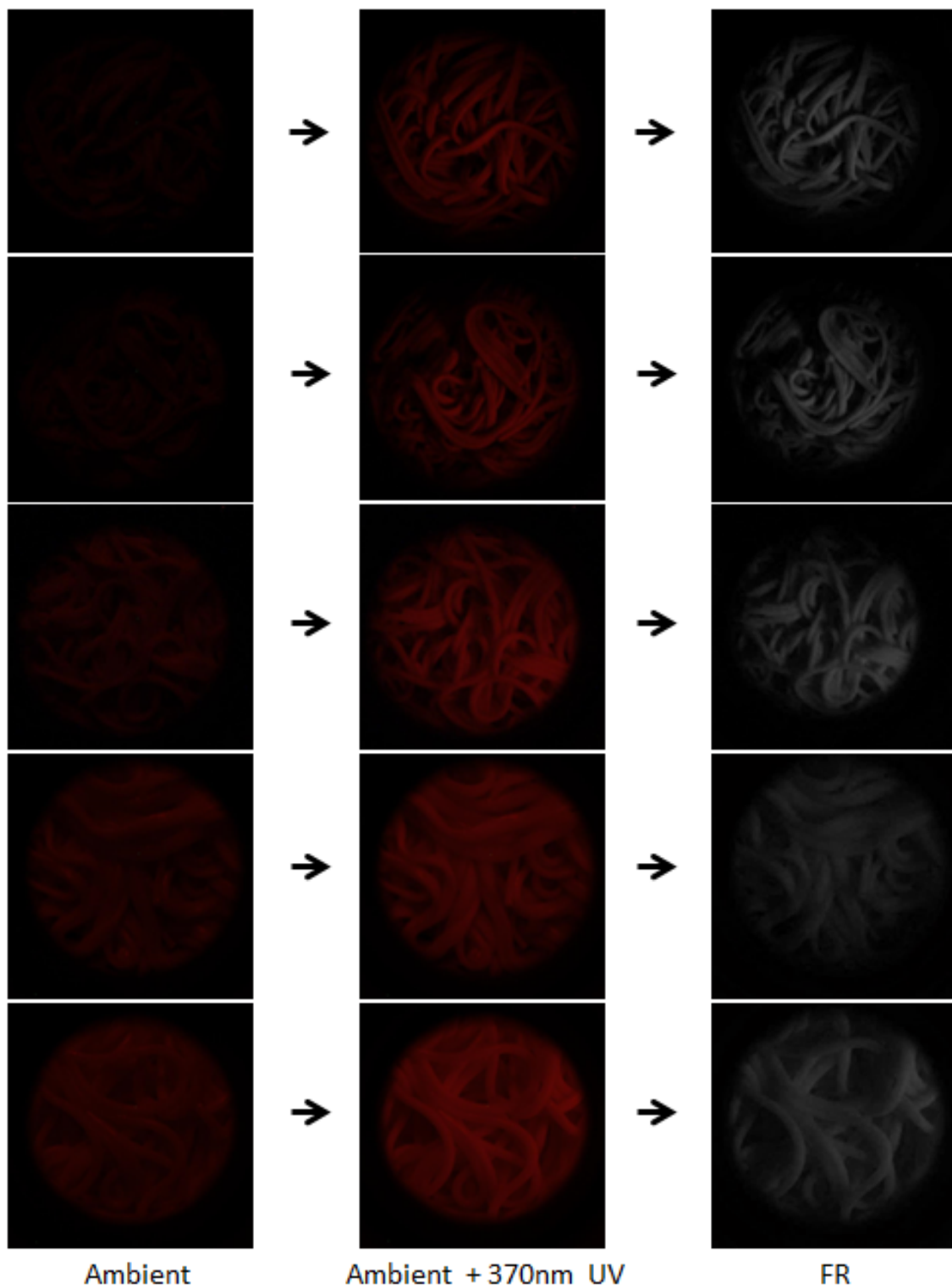


Figure 5.8: Images of boiled noodles taken at 650nm. From top to bottom: 100% buckwheat noodle, 80% buckwheat noodle, 50% buckwheat noodle, Udon and Pasta. Images in the left column were taken under ambient light, while the middle column were taken under ambient and UV light.

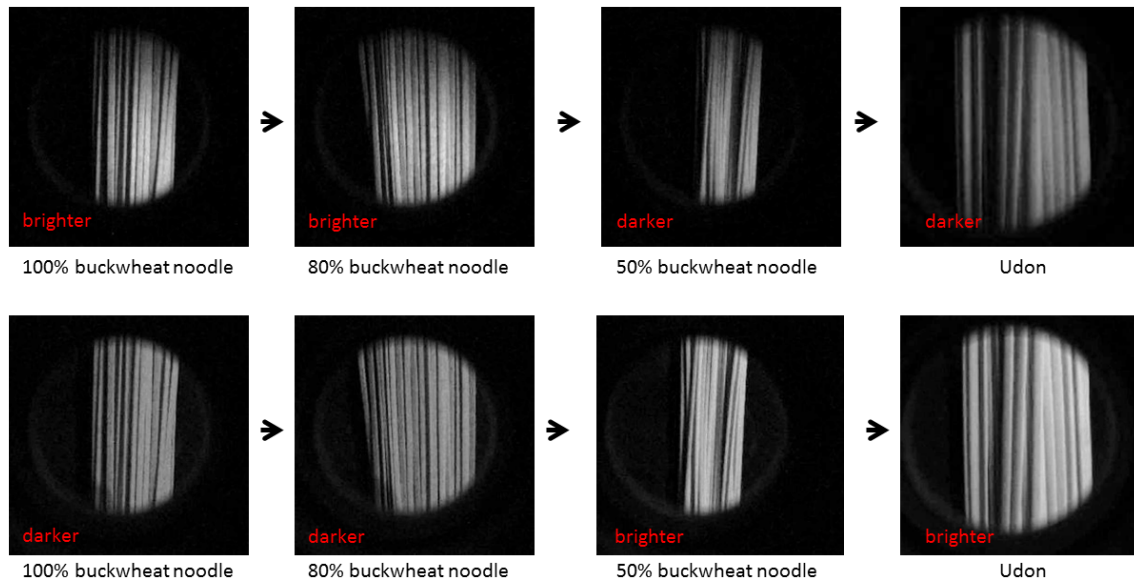


Figure 5.9: Fluorescence images of dried noodles taken at 650 nm. Images in the top row were taken by using 370 nm UV light source, while images in the second row were taken by using ordinary blue light.

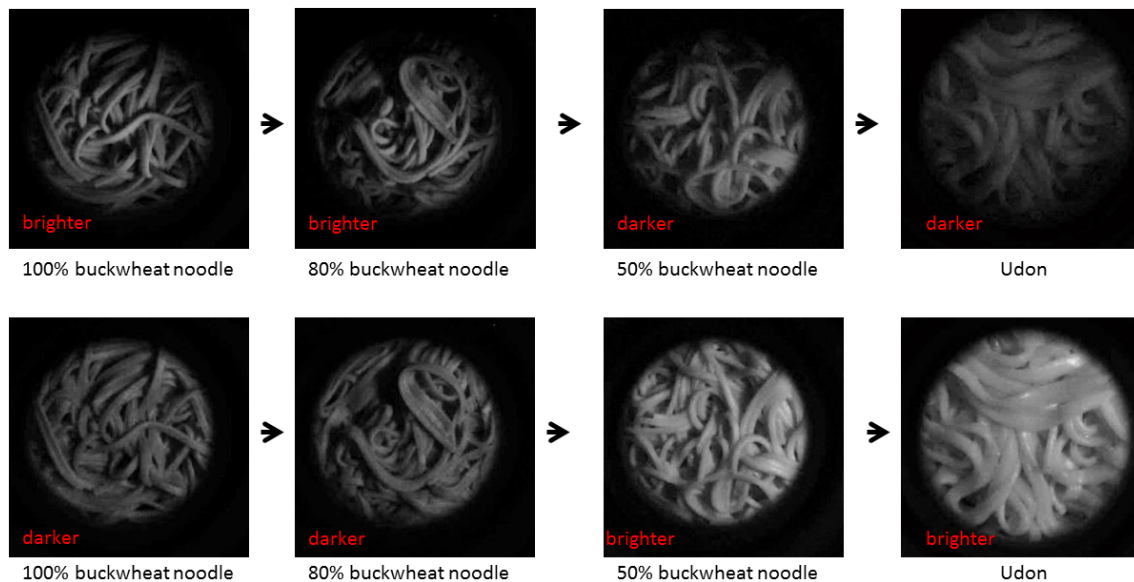


Figure 5.10: Fluorescence images of boiled noodles taken at 650 nm. Images in the top row were taken by using 370 nm UV light source, while images in the second row were taken by using ordinary blue light.

Chapter 6

Conclusion

6.1 Summary

We have proposed a method for food quality measurement based on digital fluorescence image. According to the Excitation-Emission spectra (or EEM) of a few primary fluorophores in food, we chose corresponding UV light as light source, then took photos at a series of selected wavelengths, through which we caught the fluorescence of target fluorophores in food successfully. At last, we used Partial Least Square Regression (PLSR) to build a model to predict food quality.

Our basic idea is to get fluorescence images at the most effective wavelength, because different kinds of food have different EEM. For meat, the most useful fluorescence image should be caught in the middle range of visible wavelengths, which is contributed by tryptophan and NADH. While for mixture of wheat and buckwheat flours, we had better take photos at a few wavelengths distribute from 400 nm to 700 nm if we want to detect and estimate buckwheat ratio. After getting fluorescence images, we can extract proper features to predict food quality.

Experimental results showed that our method worked well for predicting buckwheat flour ratio. Compared with hundreds of dimensions of EEM, we got an acceptable prediction result ($R^2 = 0.986679$ and $SEP = 0.131205$) by using only 6 wavelengths, which is very simple and rapid. We also observed the fluorescence of buckwheat from both dried and boiled buckwheat noodles at 650 nm, which means that using our method to predict buckwheat content in commercial noodles is possible.

Although we only did a simple prediction on buckwheat flour ratio of flour mixture, our work proved that fluorescence image based method is a simple and rapid method to estimate food quality compare with EEM.

6.2 Discussion and Future Works

In this work, we gave up predicting meat quality although we have already got fluorescence images from meat successfully, because meat has too many quality indicators and it is difficult for us to get the ground truth of these indicators in the lab. So we finally shifted to buckwheat flour products which are easy to get the real quality value, and predict buckwheat flour ratio by using fluorescence image successfully. However, we can see obvious changes from the fluorescence images of meat as meat goes bad day by day. That means a high correlation between meat and its fluorescence. So it is possible to estimate meat quality through fluorescence images if we chose proper features and had a method to get the ground truth of quality indicators such as freshness.

For future work, there are still a few remaining issues to be solved. We list up our recommendation for future works as following, in no particular order.

- **Estimation of buckwheat ratio in commercial buckwheat products**

By using filters in front of camera and light source, we observed fluorescence from both dried and boiled buckwheat noodles at 650 nm. This gave us an inspiration that we could realize the visualization of buckwheat component in many kinds of commercial products with buckwheat in them. Moreover, fluorescence images taken at a few selected wavelengths can also be used to predict buckwheat content in these commercial products. 650 nm is thought to be one of the most important wavelengths.

- **Estimation of meat quality**

Meat has a lot of quality indicators such as freshness, tenderness, fat content and so on. Different quality indicators may be highly correlated to different fluorophores in meat, and be reflected by fluorescence images taken under different wavelengths. So many work can be done on estimating meat qualities by using fluorescence image based method.

- **Estimation of the proportion of primary fluorescent components in meat**

We also can try to use fluorescence image based method to estimate the ratio of different fluorophores in meat. Either band-pass filters or variable light source can be used to collect data, then build equation sets. However, the premise behind this idea is that we are clear about the primary fluorescent components in meat samples.

References

- [1] D. W. SUN, *HYPERSPECTRAL IMAGING FOR FOOD QUALITY ANALYSIS AND CONTROL*. ACADEMIC PRESS, 2010.
- [2] V.-D. T, “Synchronous luminescence spectroscopy: methodology and applicability,” *Appl Spectrosc*, vol. 36, pp. 576–581, 1982.
- [3] C. Zheng, D. W. Sun, and L. Zheng, “Recent development of image texture for evaluation of food qualities — a review,” *Trends in Food Science and Technology*, vol. 17, pp. 113–128, 2006.
- [4] C. Zheng, D.-W. Sun, and L. Zheng, “Recent developments and applications of image features for food quality evaluation and inspection — a review,” *Trends in Food Science and Technology*, vol. 17, pp. 642–655, 2006.
- [5] G. ElMasry, D.-W. Sun, and P. Allen, “Non-destructive determination of water-holding capacity in fresh beef by using nir hyperspectral imaging,” *Food Research International*, vol. 44, pp. 2624–2633, 2011.
- [6] Y. Fu, A. Lam, I. Sato, T. Okabe, and Y. Sato, “Separating reflective and fluorescent components using high frequency illumination in the spectral domain,” *International Conference on Computer Vision (ICCV)*, 2013.
- [7] S. Moser, A. Muller, T. Holzinger, C. Lutz, S. Jockusch, N. J. Turro, and B. Krautler, “Fluorescent chlorophyll catabolites in bananas light up blue halos of cell death,” *Proceeding of the National Academy of Sciences*, vol. 106, pp. 15538–15543, 2009.
- [8] G. Gremaud, S. Karlen, and K. Hulliger, “Analytical methods for the authentication of meat and meat products: recent developments,” *Mitteilungen aus Lebensmitteluntersuchung und Hygiene*, vol. 93, pp. 481–502, 2002.
- [9] N. Ballin and R. Lametsch, “Analytical methods for authentication of fresh vs. thawed meat — a review,” *Meat Science*, vol. 80, pp. 151–158, 2008.
- [10] M. Shibata, K. Fujita, J. Sugiyama, M. Tsuta, M. Kokawa, Y. Mori, and H. Sakabe, “Predicting the buckwheat flour ratio for commercial dried buckwheat noodles based

References

- on the fluorescence fingerprint,” *Biosci. Biotechnol. Biochem*, vol. 75, pp. 1312–1316, 2011.
- [11] P. Sale, “Increase in the electric conductivity of meats following the freezing-thawing process,” *Comptes rendus hebdomadaires des seances de l’Academie des sciences. Serie D: Sciences naturelles*, vol. 269, no. 5, pp. 2136–2139, 1969.
- [12] P. Gottesmann and R. Hamm, “Development of an enzymatic method to differentiation between fresh meat and frozen thawed meat,” *Zeitschrift fu?r Lebensmittel-Untersuchung und -Forschung*, vol. 184, pp. 115–121, 1987.
- [13] G. ELMASRY, D. F. BARBIN, D.-W. SUN, and P. ALLEN, “Meat quality evaluation by hyperspectral imaging technique: An overview,” *Critical Reviews in Food Science and Nutrition*, vol. 52, pp. 689–711, 2012.
- [14] S. Cubero, N. Aleixos, E. Molto, J. G ´omez Sanchis, and J. Blasco, “Advances in machine vision applications for automatic inspection and quality evaluation of fruits and vegetables,” *Food and Bioprocess Technology*, vol. 4, pp. 487–504, 2011.
- [15] G. ElMasry and J. Wold, “High-speed assessment of fat and water content distribution in fish fillets using online imaging spectroscopy,” *Journal of Agricultural and Food Chemistry*, vol. 56, pp. 7672–7677, 2008.
- [16] R. Lu and Y. Chen, “Hyperspectral imaging for safety inspection of food and agricultural products,” *SPIE Conference on Pathogen Detection and Remediation for Safe Eating*, vol. 3544, pp. 121–133, 1998.
- [17] G. Bonifazi and S. Serrati, “Hyperspectral imaging applied to complex particulate solids systems,” *Proceeding of SPIE*, vol. 7003, p. 70030F, 2008.
- [18] D. Ariana and R. Lu, “Detection of internal defect in pickling cucumbers using hyperspectral transmittance imaging,” *Transactions of the ASABE*, vol. 51, pp. 705–713, 2008.
- [19] R. Karoui and C. Blecker, “Fluorescence spectroscopy measurement for quality assessment of food systems—a review,” *Food Bioprocess Technol*, vol. 4, pp. 364–386, 2011.
- [20] D.W.Johnson, J.B.Callis, and G.D.Christian, “Rapid scanning fluorescence spectroscopy,” *ANALYTICAL CHEMISTRY*, vol. 49, no. 8, p. 757A, 1977.
- [21] T. Sugiyama, K. Fujita, M. Tsuta, and J. Sugiyama, “Prediction for mixture rate of buckwheat flour against wheat flour using excitation-emission matrix (eem),” *Nippon Shokuhin Kagaku Kogaku Kaishi*, vol. 57, no. 6, pp. 238–242, 2010.

References

- [22] M. Tsuta, K. Miyashita, T. Suzuki, S. Nakauchi, Y. Sagara, and J. Sugiyama, “Three-dimensional visualization of internal structural changes in soybean seeds during germination by excitation-emission matrix imaging,” *Trans. ASABE*, vol. 50, pp. 2127–2136, 2007.
- [23] M. Kokawa, K. Fujita, J. Sugiyama, M. Tsuta, M. Shibata, T. Araki, and H. Nabetani, “Visualization of gluten and starch distributions in dough by fluorescence fingerprint imaging,” *Biosci. Biotechnol. Biochem*, vol. 75, pp. 2112–2118, 2011.
- [24] C. J. Du and D. W. Sun, “Recent development in the applications of image processing techniques for food quality evaluation,” *Trends in Food Science and Technology*, vol. 15, pp. 230–249, 2004.
- [25] B. Bennedsen, D. Peterson, and A. Tabb, “Identifying defects in images of rotating apples,” *Computers and Electronics in Agriculture*, vol. 48, pp. 92–102, 2005.
- [26] V. Leemans and M. Destain, “A real-time grading method of apple based on features extracted from defects,” *Journal of Food Engineering*, vol. 61, pp. 83–89, 2004.
- [27] Y. Huang, R. Lacey, L. Moore, R. Miller, A. Whittaker, and J. Ophir, “Wavelet textural features from ultrasonic elastograms for meat quality prediction,” *Transactions of the ASAE*, vol. 40, pp. 1741–1748, 1997.
- [28] A. Thybo, P. Szczypiński, A. Karlsson, S. Donstrup, H. S. Jorgensen, and H. Andersen, “Face synthesis prediction of sensory texture quality attributes of cooked potatoes by nmr-imaging (mri) of raw potatoes in combination with different imaging analysis methods,” *Journal of Food Engineering*, vol. 61, pp. 91–100, 2004.
- [29] E. Cernadas, P. Carrion, P. Rodriguez, E. Muriel, and T. Antequera, “Analyzing magnetic resonance images of iberian pork loin to predict its sensorial characteristics,” *Computer Vision and Image Understanding*, vol. 98, pp. 345–361, 2005.
- [30] A. Ghazanfari and J. Irudayaraj, “Classification of pistachio nuts using a string matching technique,” *Transactions of the ASAE*, vol. 39, pp. 1197–1202, 1996.
- [31] R. Haralick, R. Shanmugam, and I. Dinstein, “Absorption spectra textural features for image classification,” *IEEE Transactions on System, Man, and Cybernetics*, vol. 3, pp. 610–621, 1973.
- [32] M. Amadasun and R. King, “Textural features corresponding to textural properties,” *IEEE Transactions on Systems, Man, and Cybernetics*, vol. 19, pp. 1264–1274, 1989.
- [33] J. Tan, “Meat quality evaluation by computer vision,” *Journal of Food Engineering*, vol. 61, pp. 27–35, 2004.

References

- [34] I. Hatem, J. Tan, and D. Gerrard, "Determination of animal skeletal maturity by image processing," *Meat Science*, vol. 65, pp. 999–1004, 2003.
- [35] G. Jahns, H. Nielsen, and W. Paul, "Measuring image analysis attributes and modelling fuzzy consumer aspects for tomato quality grading," *Computers and Electronics in Agriculture*, vol. 31, pp. 17–29, 2001.
- [36] X. Cheng, Y. Chen, Y. Tao, C. Wang, M. Kim, and A. Lefcourt, "A novel integrated pca and fld method on hyperspectral image feature extraction for cucumber chilling damage inspection," *Transactions of the ASAE*, vol. 47, pp. 1313–1320, 2004.
- [37] I. Kim, M. Kim, Y. Chen, and S. Kong, "Detection of skin tumors on chicken carcasses using hyperspectral fluorescence imaging," *Transactions of ASAE*, vol. 47, pp. 1785–1792, 2004.
- [38] C. Yang, K. Chao, and Y. Chen, "Development of multispectral image processing algorithms for identification of wholesome, septicemic, and inflammatory process chickens," *Journal of Food Engineering*, vol. 69, pp. 225–234, 2005.
- [39] D. Barbin, G. Elmasry, and D. W. Sun, "Nir hyperspectral imaging for fat quantification in minced pork,"
- [40] Q. Jun, M. Ngadi, and N. Wang, "Pork quality classification using a hyperspectral imaging system and neural network," *International Journal of Food Engineering*, vol. 3, 2007.
- [41] K. Nishino, K. Nakamura, and M. Tsuta, "Optimization of excitation-emission band-pass filter for visualization of viable bacteria distribution on the surface of pork meat," *Optics express*, vol. 21, pp. 12579–12591, 2013.
- [42] D. A. Skoog, F. J. Holler, and S. R. Crouch, *Principles of Instrumental Analysis*. Thomson Publishers, 2007.
- [43] S. Tominaga and E. Takahashi, "Spectral image processing by a multi-channel camera," *ICIP*, vol. 99, pp. 575–579, 1999.
- [44] C. Zhang and I. Sato, "Separating reflective and fluorescent components of an image," *IEEE Conference on Computer Vision and Pattern Recognition (CVPR)*, 2011.
- [45] S. Moser, T. Muller, and M. O. Ebert, "Blue luminescence of ripening bananas," *Angewandte Chemie International Edition*, vol. 47, pp. 8954–8957, 2008.
- [46] J. R. Lakowicz, *Principles of Fluorescence Spectroscopy*. Springer Science+Business Media, LLC, 2006.

References

- [47] S. G. Schulman, "Molecular luminescence spectroscopy: methods and applications," *Wiley-Interscience*, vol. 1, 1985.
- [48] J. Christensen, L. Norgaard, R. Bro, and S. B. Engelsen, "Multivariate autofluorescence of intact food systems," *Chemical Reviews*, vol. 106, no. 6, 2006.
- [49] *Food Fluorescence Library*, 2005.
- [50] S. I. P. BIOCITECH, "Fluorescence as an indicator of raw food quality, food processing severity and storage impact," 2012.
- [51] S. A. Jensen, S. Reenberg, and L. Munck, "Fluorescence analysis in fish and meat technology," *Fluorescence analysis in foods*, pp. 181–192, 1989.
- [52] J. P. Frencia, E. Thomas, and E. Dufour, "Measure of meat tenderness using front face fluorescence spectroscopy," *Science des Aliments*, vol. 23, pp. 142–145, 2003.
- [53] K. M. Davitt, *Ultraviolet Light Emitting Diodes and Bio-aerosol Sensing*. Brown University, 2006.
- [54] H. J. Swatland, "Autofluorescence of adipose tissue measured with fibre optics," *Meat Science*, vol. 19, pp. 277–284, 1987.
- [55] H. Swatland and S. Barbut, "Fluorimetry via a quartz glass rod for predicting the skin content and processing characteristics of poultry meat slurry," *International journal of food science and technology*, vol. 26, pp. 373–380, 1991.
- [56] H. J. Swatland and S. Barbut, "Optical prediction of processing characteristics of turkey meat using uv fluorescence and nir birefringence," *Food research international*, vol. 28, pp. 227–232, 1995.
- [57] H. J. Swatland, T. Nielsen, and J. R. Andersen, "Correlations of mature beef palatability with optical probing of raw meat," *Food research international*, vol. 28, pp. 403–416, 1995.
- [58] H. J. Swatland, E. Gullett, and T. Hore, "Uv fiber-optic probe measurements of connective tissue in beef correlated with taste panel scores for chewiness," *Food research international*, vol. 28, pp. 23–30, 1995.
- [59] H. J. Swatland and C. J. Findlay, "On-line probe prediction of beef toughness, correlating sensory evaluation with fluorescence detection of connective tissue and dynamic analysis of overall toughness," *Food quality and preference*, vol. 8, pp. 233–239, 1997.

References

- [60] K. I. Hildrum, J. P. Wold, V. H. Segtnan, and J. P. Renou, "New spectroscopic techniques for online monitoring of meat quality," *Advanced technologies for meat processing*, pp. 88–129, 2006.
- [61] B. Egelanddal, K. Kvval, and T. Isaksson, "Autofluorescence spectra as related to tensile properties for perimysium from bovine masseter," *Journal of food science*, vol. 61, pp. 342–347, 1996.
- [62] J. Brondum, L. Munck, and P. Henckel, "Prediction of water-holding capacity and composition of porcine meat by comparative spectroscopy," *Meat Science*, vol. 55, pp. 177–185, 2000.
- [63] I. Allais, E. Dufour, and A. e. a. Pierre, "Monitoring the texture of meat emulsions by front-face fluorescence spectroscopy," *Sciences des aliments*, vol. 23, pp. 128–131, 2003.
- [64] I. Allais, C. Viaud, and e. a. Pierre, A, "A rapid method based on front-face fluorescence spectroscopy for the monitoring of the texture of meat emulsions and frankfurters," *Meat Science*, vol. 67, pp. 219–229, 2004.
- [65] A. Veberg, *Fluorescence spectroscopy of food lipid oxidation*. PhD thesis, Norwegian University of Life Science, Norway, Norwege, 2006.
- [66] J. P. Wold and M. Mielnik, "Nondestructive assessment of lipid oxidation in minced poultry meat by autofluorescence spectroscopy," *Journal of food science*, vol. 65, pp. 87–95, 2000.
- [67] W. J. P, M. M, and P. M. K, "Rapid assessment of rancidity in complex meat products by front face fluorescence spectroscopy," *Journal of food science*, vol. 67, pp. 2397–2404, 2002.
- [68] N. Oto, S. Oshita, Y. Makino, Y. Kawagoe, J. Sugiyama, and M. Yoshimura, "Non-destructive evaluation of atp content and plate count on pork meat surface by fluorescence spectroscopy," *Meat Science*, vol. 93, pp. 579–585, 2013.